Journal of Medicinal Chemistry

Article

Are We There Yet? – Applying Thermodynamic and Kinetic Profiling on Embryonic Ectoderm Development (EED) Hit-to-Lead Program

Ying Wang, Rohinton P. Edalji, Sanjay C. Panchal, Chaohong C. Sun, Stevan W Djuric, and Anil Vasudevan

J. Med. Chem., **Just Accepted Manuscript** • DOI: 10.1021/acs.jmedchem.7b00576 • Publication Date (Web): 19 Sep 2017

Are We There Yet? – Applying Thermodynamic and Kinetic Profiling on Embryonic Ectoderm Development (EED) Hit-to-Lead Program

*Ying Wang**[‡], Rohinton P. Edalji [‡], Sanjay C. Panchal [‡], Chaohong Sun, Stevan W. Djuric and Anil Vasudevan*

AbbVie Inc., 1 North Waukegan Road, North Chicago, Illinois 60064, United States

[‡] These authors contributed equally

KEYWORDS. Structure-Kinetics Relationship, Structure-Thermodynamics Relationship, EED, ITC, k_{off} , k_{on}, enthalpy, entropy, SPR

ABSTRACT. It is advocated that kinetic and thermodynamic profiling of bioactive compounds should be incorporated and utilized as complementary tools for hit and lead optimizations in drug discovery. To assess their applications in the EED hit-to-lead optimization process, large amount of thermodynamic and kinetic data were collected and analyzed via isothermal titration calorimetry (ITC) and surface plasmon resonance (SPR), respectively. Slower dissociation rates (k_{off}) of the lead compounds were observed as the program progressed. Analysis of the kinetic data indicated that compound cellular activity correlated with both K_i and k_{off}. Our analysis

revealed that ITC data should be interpreted in the context of chiral purity of the compounds. The thermodynamic signatures of the EED amino pyrrolidine compounds were found to be mainly enthalpy driven with improved enthalpic contributions as the program progressed. Our study also demonstrated that significant challenges still exist in utilizing kinetic and thermodynamic parameters for hit selection.

INTRODUCTION

Drug discovery is a complex process in which multiple factors of bioactive compounds need to be optimized in parallel to lead to a clinical candidate with balanced efficacy and selectivity. For nearly a century, the binding affinity of a compound for the target of interest has been one of the major guiding principles in drug discovery, coined by Paul Ehrlich in 1913, "Substances do not act unless bound". However, it has also been long recognized that binding affinity alone is not sufficient to predict a successful clinical outcome. As such, a number of metrics focusing on the a compound's characteristics, such as Lipinski rule of five and its variants, have been correlated to clinical observations, and subsequently incorporated routinely in the hit and lead optimization processes.[1] As we continued to look for better or complementary principles to guide drug discovery efforts, we became aware of studies that discuss the importance of incorporating binding kinetics and thermodynamics into drug discovery compound triage over the last decade. It has been proposed that efficacy and selectivity may also be driven by kinetics and thermodynamics, often overlooked dimensions in conventional SAR profiling.[2,3,4,5]

Association and dissociation rate constants (k_{on} and k_{off}) of a compound binding to a biological target are not intrinsically related to one another, although they are connected by dissociation

equilibrium constant K_D ($K_D = k_{off}/k_{on}$). In theory, they are correlated with the structural elements of the compound-protein complex during the association and dissociation processes.[6,7] The kinetic profile of structurally different compounds could reveal features and aspects of compound-protein interactions and thus aid optimization. This is defined as structure-kinetics relationships (SKR). It is postulated that in many cases, k_{off} is a better predictor for *in vivo* efficacy and selectivity, and has the potential to differentiate otherwise indistinguishable compounds with similar affinities.[8,9]

Similarly, the relative contribution of the binding enthalpy ΔH and entropic term -TΔS of a compound is claimed to be of importance to predict its selectivity in clinical studies. [10,11] Structure-thermodynamics relationships (STR) could be defined in theory as well. A large negative value of ΔH is believed to be desirable as it reflects the strength of specific compound-ligand interactions such as hydrogen bonds, while large negative entropic term -TΔS mainly reflects nonspecific lipophilic interactions.

Recommendations were thus made that a more holistic approach including binding kinetic and thermodynamic data should be incorporated as early as possible in the drug discovery process. It has been claimed that this may enable medicinal chemists to identify and prioritize hit and lead compounds with best-in-class potentials. [2,3,4,5] However, many of these claims were rationalized from retrospective analyses of drugs in the clinic, giving little guidance on their utilization in the hit and lead optimization processes. In addition, there exists a lack of thermodynamic and kinetic data in the drug discovery phase to sustain many of the underlying assumptions. General validation of these claims remains to be established. In fact, some of the claims are not without controversies and have been challenged by several recent articles.[12, 13] The proposed impact of

binding kinetics and thermodynamics that will ultimately lead to clinical candidates, is yet to be demonstrated.[14] To gauge the applications of thermodynamic and kinetic profiling in drug discovery, we decided to investigate these parameters in a hit-to-lead medicinal chemistry program.

Polycomb repressive complex 2 (PRC2) catalyzes trimethylation of histone H3 at lysine 27 (H3K27me3).[15] It plays an essential role in gene regulation and is a known epigenetic drug target for cancer therapy. EZH2 (enhancer of zeste homolog 2) is the catalytic subunit of PRC2 that is responsible for histone methylation. As such, EZH2 has received a lot of attention within the pharmaceutical industry as a potential drug target. To date, a number of small molecule EZH2 inhibitors have been developed and advanced into cancer clinical trials.[16] EED (embryonic ectoderm development), another core component of PRC2, is at least partially responsible for the recognition of H3K27me3. The direct association of the PRC2 complex to histone H3K27me3 through EED stimulates the successive methyltransferase activity of PRC2, which results in the propagation of the H3K27me3 histone mark and silencing of target genes through generation of repressed chromatin. Therefore, blocking this process allosterically via inhibiting the H3K27me3 binding function of EED seems to be an attractive approach for cancer therapy. Indeed, we and Novartis have very recently disclosed novel EED inhibitors that demonstrated robust efficacy against human tumor xenograft models.[17,18]

Our medicinal chemistry efforts started with the identification of amino pyrrolidine compound **1** from a high throughput thermal shift assay (TSA) based screen (Figure **1**).[19] Compound **1** was confirmed by EED TR-FRET assay with a K_i of 600 nM. The X-ray crystal structure of EED WD40 domain with compound **1** at 1.28 Å suggested that compound **1** bound in the histone peptide binding site of EED. Interestingly, when compared to the previously published structure

of EED binding the H3K27mes peptide, significant remodeling of the peptide binding pocket to accommodate compound **1** was observed, despite similar global binding of peptide and compound **1** to EED.[17] Both Trp364 and Tyr365 flipped up to expose a larger and more druggable binding pocket that allowed the 2-methoxybenzyl group to slide deep into the hydrophobic pocket (Figure **2a**). Additional key interactions included a hydrogen bond from the dimethylamino group to highly coordinated water. This dimethylamino moiety is, thus, largely non-replaceable (Figure **2b**). Other interactions include the hydrophobic and van der Waals interactions between the rings of the indole and protein. The initial complex structure suggested that the both the indole (R_1) and N-benzyl moieties (R_2) in compound **1** would be amenable for SAR studies (Figure **3**).[19]

The study of structure-kinetics and structure-thermodynamics relationships (SKR and STR), needless to say, will be most fruitful when considering analogs within a specific chemical series for a given target. The availability of the high resolution x-ray structures and biophysical confirmation methods, coupled with synthetic tractability of the amino pyrrolidine series prompted us to study the SKR and STR at the onset of EED hit-to-lead program. This case study was aimed at gauging the feasibility of applying kinetic and thermodynamic information for the prospective design in the hit-to-lead optimization stage.

RESULTS AND DISCUSSION

DATASET. About one hundred amino pyrrolidine EED inhibitors were profiled in ITC and SPR assays in addition to EED TR-FRET assay. These analogs were carefully selected to cover a broad range of biochemical affinities (K_i = 0.0005 μM to 50 μM). Analogs with chemical

structural variations were systematically selected and included in the dataset (Figure **3**). Data from cellular assays that measured selective inhibition of H3K27 trimethylation and proliferation in tumor cell lines were collected on half of the compounds. X-ray crystal structures were obtained on twenty percent of the compounds. This represents one of the most comprehensive thermodynamic and kinetic profiling datasets in the literature that focuses on one chemical series for one target.

STRUCTURE-KINETICS RELATIONSHIP. A Biacore T200 was used to collect the compound binding data. EED (h) (78-441) was minimally biotinylated and captured on a neutravidin surface for all SPR binding studies. Compounds were then assayed in the SPR runs. As per manufacturer guidance, the detection ranges of the SPR used in our study are k_{on} 10^3-10^7 $M^{-1}s^{-1}$and k_{off} 10^{-5}- 0.5 s^{-1}, respectively. Roughly 25% of the EED compounds studied had both fast k_{on} ($>10^7$ $M^{-1}s^{-1}$) and k_{off} (> 0.5 s^{-1}) rates that were beyond our biacore detection limit. In these cases, steady-state K_D values were obtained instead and ranged from 8 nM to 50 μM.

The k_{on} values spanned more than three log unit, from 4.2×10^3 to > 1×10^7 $M^{-1}s^{-1}$. Similarly, the k_{off} spanned more than two log units, from 7×10^{-4} to > 0.5 s^{-1}. Our data clearly showed that k_{on} could vary dramatically even among close analogs. Recent literature examples suggested in certain cases k_{on} may also play an important role in downstream processes.[20,21]

The binding affinities determined from SPR studies, K_D, correlated well with the binding affinities, K_i, obtained from our TR-FRET biochemical assay (Figure **4**). The SPR data, thus, directly validated the binding affinity K_i readout from our EED TR-FRET assay.

From the SAR studies, the R_2 group, where the original 2-methoxybenzyl group in compound **1** was at, had a strong preference for 2,6-disubstitution (Figure **3**). This led to the discovery of 2-

bromo-6-fluorobenzyl (**A**) as the initial preferred R_2 group. More than half of the compounds profiled in SPR were analogs based on R_2 as **A** while variation in R_1 groups helped map out the initial SAR. From the X-ray structures, the R_1 group projected out towards water-exposed EED protein and was considered to potentially accommodate a variety of substituents. In practice, many aryl and heteroaryl groups were tolerated at the R_1 position and afforded potent EED amino pyrrolidine analogs.

Extensive analoging via parallel library synthesis in efforts to find other suitable R_2 groups led to the discovery of 2-fluoro-6-methylbenzyl (**B**) analogs. These analogs generally had equal or improved potency to the 2-bromo-6-fluorobenzyl analogs (**A**), but the 2-fluoro-6-methylbenzyl (**B**) also had much better overall physicochemical properties (Figure **3**). A handful of these compounds were profiled in SPR binding measurements with optimal R_1 groups identified from earlier SAR studies.

As the project progressed, based on X-ray crystal structures, we reasoned that restricting the conformational freedom of the benzyl moiety at the R_2 position may enforce the favorable binding conformation observed in the X-ray structures.[19] This led to the identification of the 7-fluoro-2-indanyl group at the R_2 position (**C**, Figure **3**). Fine tuning of the R_1 group eventually led to the discovery of compound **2** as the lead compound, which provided on-target tumor growth inhibition in a mouse xenograft model (Figure **1**).[19]

The kinetic plot of the compounds with these three different R_2 groups is shown in Figure **5**. Compounds with fast k_{on} or k_{off} were not depicted in Figure **5**. Slower k_{off} values were observed generally when R_2 progressed from **A** to **B** then to **C**. However, no such trend was observed for k_{on} for this R_2 progression. Instead, a similar range of k_{on} values were observed going from **B** to

C. The broader coverage of k_{on} and k_{off} values of analogs with R_2 = **A** was as expected as we used R_2 = **A** to map out the SAR at R_1 at the beginning of the hit to lead program. This broader coverage was also reflected in the wider range of the K_D values with R_2 = **A** (Figure **5**). As the program progressed, K_D and k_{off} were simultaneously improved for the EED amino pyrrolidine series. This trend was also observed when comparing matched pairs, such as compound **3** vs **4** and compound **5**, **6** vs **7** (Table **1**), where the trend of k_{off} values tracked the binding affinity K_D trend, although not linearly.

Without sufficient detailed knowledge to unravel all of the binding events that happened during the formation of the protein-compound complex, especially information on the transition states in the complex formation process, we did not attempt to quantify the observed phenomenon. Yet, we hypothesized that the optimal interactions between the rigid indanyl group and the hydrophobic protein pocket as evidenced from the static X-ray structures were likely responsible for the observed slower k_{off} in the 7-fluoroindanyl analogs.

Enantiomers with the (3R, 4S) configuration were preferred for the R_2 groups studied, generally several fold more potent than the corresponding enantiomers with the (3S, 4R) configurations. Compound **8**, the less potent enantiomer, had fast k_{on} and k_{off} rates. The more potent enantiomer **9** though, had slower measurable k_{on} and k_{off}. A similar trend was observed for compound **10** and **11**. This indicated that enantiomers can have very different kinetic signatures despite their structural similarities.

In our case, the effect of the polar group on kinetic parameters depended on its position and interaction within the X-ray structure. Compound **12**, lacked a hydroxyl group at the R_1 position compared to compound **13**, but showed similar binding affinity. Both compounds had fast k_{on}

and k_{off} rates. Compound **14,** with a polar substituent at R_1, a pyridyl group, also had fast k_{on} and k_{off} rates. On the contrary, comparing compound **15** to compound **16**, which differs by a hydroxyl group at R_2 position, the k_{on} was largely unchanged while the k_{off} differed by several fold. From X-ray structures of similar analogs, we knew that the hydroxyl group at the *para* position on the benzyl substituent at the R_2 position, such as in compound **16**, forms an H-bond to the carbonyl of Asp310 in the protein complex. This could at least partially explain the slower k_{off} observed. In contrast, the hydroxyl group of compound **13** is projected out towards the water-exposed EED protein without forming a hydrogen bond with the EED protein, and one would expect little influence on the kinetic parameters.

A proliferation assay featuring the Pfeiffer (human lymphoblast) tumor cell line was used to evaluate the inhibition of EED by the amino pyrrolidine compounds. The IC_{50} of the amino pyrrolidine EED compounds from this cellular assay were binned into three categories: IC_{50} less than 0.1μM, more than 1μM and IC_{50} in between. From the box plots in Figure **6**, the cellular activity improved with improved median value of K_i from the TR-FRET assay (Figure **6a**). We also noticed a correlation between slower k_{off} and improved cellular activity (Figure **6b**). On the contrary, the trend was much less obvious with k_{on} (Figure **6c**). The median value for k_{on} only increased slightly with improved cellular activity. It should be pointed out that although the k_{off} values could potentially be used to predict cellular activity, the same conclusion could also be reached by using the binding affinity K_i from the TR-FRET assay in our case. The lead compound identified (compound **2**), had the best cellular activity, and the best K_i and the slowest k_{off} value of all the compounds tested, but not the fastest k_{on}.

We also investigated if there was any correlation between kinetic parameters (k_{on} and k_{off}) and physicochemical parameters. The wide physicochemical parameter distribution of amino

pyrrolidine series in the hit-to-lead stage (e.g. MW 333- 533, ClogP 1.8 - 6.4 and tPSA 5-67) made such an analysis feasible. No correlation could be found in our case. However, it has been previously reported that a correlation exists between the k_{off} and the molecular weight of compounds.[22] The correlation though was derived from a study of compounds for more than 40 targets. It is plausible, in our case, that local effects of a specific structural moiety in the context of the protein target of interest could be dominant over the physicochemical descriptors in influencing kinetic signatures. The lack of correlation with physicochemical parameters in our case also indicated that kinetic signatures could be considered as independent parameters in the compound optimization process.

It was proposed that kinetic profiling could be used to distinguish and prioritize chemical series in the early stage of the medicinal chemistry programs. The idea was put forward that hits with slower k_{off} values should be prioritized for further optimization. To test this claim, hits identified from our EED HTS campaign were also profiled in the SPR binding. Selected examples were given in Table **1** (entry **1**, **17** and **18**). The majority of the initial EED HTS hits identified in our case possessed fast k_{on} and k_{off} rates. This is not surprising as the initial hits identified from HTS in general were not designed specifically for the target of interest, thus the compounds were not optimized to display optimal kinetic profiles for the EED target. Based on our experience, it is very common for the initial HTS hits of a given target to have fast k_{on} and k_{off} values.

Furthermore, compound **1** was the original pyrrolidine EED hit with fast k_{on} and k_{off} rates. Many analogs designed based on compound **1** continued to possess fast k_{on} and k_{off} rates. Thus we were not able to use the kinetic parameters for initial compound selection. In order to fully explore the potential utility of kinetic parameters in hit-to-lead stage, further advances in instrumentation technology for kinetic measurements are warranted.

STRUCTURE-THERMODYNAMICS RELATIONSHIP. It has been proposed that enthalpy optimization maximizes the influence of forces other than hydrophobicity and compounds with more favorable enthalpy contribution will likely exhibit better efficacy and selectivity in clinical trials from retrospective analysis.[4,5] It has also been shown that in general, medicinal chemistry programs optimize binding affinities via entropy optimization by increasing the hydrophobicity of the compounds through the hit and lead optimization processes. As such, it is advocated that hits with more enthalpic contribution to affinity should be prioritized at the early stage of the medicinal chemistry campaign, as entropic optimization will likely dominate during the hit and lead optimization process.

ITC analysis is the primary technology used for directly measuring the enthalpic contribution ΔH. The binding affinity K_D is obtained from an ITC experiment via curve fitting of the binding isotherm, and consequently the entropic component ($-T\Delta S$) can be derived.

Both the enthalpic and entropic contributions of the EED compounds tested spanned more than ten log units, while the corresponding K_D from ITC experiments and K_i from TR-FRET spanned less than five log units. Globally, all the EED inhibitor tested were found to have favorable enthalpic contributions (ΔH) and unfavorable entropic contributions ($-T\Delta S$). To our surprise, there's no correlation between the K_D determined from ITC experiments and the K_i determined from the TR-FRET assay. The ratios of the K_D values from ITC experiments versus the K_i values from the TR-FRET assay scattered from less than one fold to greater than 3000 fold. The difference was especially drastic with the 7-fluoro-indanyl analogs (Figure **7**). Whilst most of the analogs with the 7-fluoro-indanyl group at R_2 position were below 10 nM in the EED TR-FRET assays, these compounds had apparent K_D values in the micromolar ranges in ITC experiments,

including lead compound **2** (Figure **7)**. The stark contrast of binding affinity values from two measurements prompted us to take a closer examination of the ITC experiments.

We set out to examine the potential influence of various ITC experimental parameters on the data readout. It is recognized that these parameters may have a profound influence on the data obtained from ITC experiments.[23,24,25] The majority of ITC experiments were done in the reverse mode. However, a few titrations in the forward mode were also carried out and confirmed the thermodynamic data obtained with reverse mode. Our ITC experiments on EED program had indicated a minimal effect of pH on the K_D values within the physiologic pH range. For this dataset all experiments were performed using the same lot of EED protein. Concentrations of the compounds tested were reconfirmed. None of these studies could explain the huge discrepancies in the binding affinities observed. Instead, these studies further confirmed and validated the original ITC experimental data we obtained. Perplexed by these observations, we took a closer look at Figure **7**, interestingly, although globally there's no correlation, the K_D from ITC experiments for compound **19** and **22** matched well with the K_i from TR-FRET (Table **2**). Contrary to our lead compound **2**, which is a mixture of two diastereomers with epimeric center at the 7-fluoroindanyl group (Figure **1**),[19] compounds **19** and **22** are enantiomers with high ee values (see experimental section).

Separation of the achiral 7-fluoroindane analogs to the individual four enantiomerically pure stereoisomers turned out to be very challenging in most cases, especially on preparative scales.[19] From a few successful chiral separations and the corresponding X-ray crystal structures, we knew the preferred stereochemistry at the three stereogenic centers, as depicted in compound **19** (Table **2**). We were able to get chiral compounds **19** and **22** in high ee values while compound **20** and **21** were contaminated with 5% of other stereoisomers. The binding affinities for Compound

19 matched well in TR-FRET, SPR and ITC experiments, as did compound **22**. In stark contrast, compounds **20** and **21**, gave measured K_D values in the micromolar range in ITC experiments even though they had measured K_i values of 3 and 42 nM respectively, in the TR-FRET assay. The achiral compound **4**, also had a K_D of 2.1 μM in ITC experiments while the measured affinities were found to be 7 nM in TR-FRET and 4 nM in SPR experiments. These results, therefore, implied that chiral purity of a compound could potentially have huge influence on the apparent K_D obtained from ITC experiments, which is not the case for TR-FRET and SPR experiments. Compound **4**, a mixture of four diastereomers, its binding affinity reflected the most potent single diastereomer, compound **19**, in SPR and TR-FRET assays, but not in ITC assay (Table **2**).

To test our hypothesis, we selected all the chiral compounds with high ee values (>95%) and looked at the K_D values of these compounds from the ITC experiments. A good correlation between the ITC K_D and TR-FRET K_i values was obtained with this subset of compounds (Figure **8**). Most of the literature reports on thermodynamic studies using ITC were studies using late stage compounds with high chiral purity or drugs on the market, as well as compounds devoid of chiral centers. The lack of a large ITC dataset on close related analogs also would make such discovery unlikely. It has also been reported recently that compound impurities could lead to pronounced changes in the measured thermodynamic parameters.[23] Here we showed that the thermodynamic readout from ITC can be further complicated by the chiral purity of the compounds of interest. This complication indicated that it would be more likely to get false negative results for binding affinities in ITC experiments compared to TR-FRET assay and SPR binding measurements, where the potency readout will reflect the most potent diastereomer within the compound tested It seems that when a compound of interest is composed of more

than one stereoisomer, albeit in small amount, simultaneous binding of the each stereoisomer to the protein in ITC experiments influence the way the instrument models the binding and handles the data analysis, which could lead to significant changes in the data readout. Advanced software for ITC data handling and more in-depth studies are needed to decipher the mechanisms behind this observed phenomenon (See Supporting Information). [26,27]

Even with this subset of 23 chirally pure compounds, huge ranges of enthalpy and entropy contributions were observed. The enthalpy component ΔH ranged from -20,100 to -11,640 cal/mol, corresponding to more than a six log unit change.[28] Similarly, the entropy component -TΔS ranged from 11,026 to 3,487 cal/mol, roughly a six log unit difference. In sharp contrast, K_D values ranged from 0.005 μM to 1.1 μM, only three log units. All amino pyrrolidine EED compounds studied had favorable enthalpic contribution and unfavorable entropic contribution. Enthalpy-entropy compensation can be clearly seen from the thermodynamic plot (Figure **9).**[25] Notably most of these analogs were observed to be in the upper left and lower right quadrants along the diagonal line in this figure. As compound optimization progressed, we observed enhanced enthalpic contributions and reduced entropic contributions to the overall binding affinity, as shown in Figure **9** from **A** to **B** to **C**.[29] This finding was also illustrated in the direct comparison of compounds **9**, **23** and **24** (Table **3**). The more than one log unit change in enthalpy from compound **9** to **23** clearly showed the potency boost came mainly from the enthalpic contribution. It is also interesting to note that although compounds **23** and **24** had similar K_D as compound progressed, the thermodynamic signatures were very different. Compound **24** had more favorable enthalpic contribution while compound **23** had much more favorable entropy contribution which offset the enthalpy difference. Although no definite answers could be

provided to explain the differences from X-ray crystal structures of these compounds alone, as the hit to lead EED project progressed, we saw dramatically improved enthalpic contribution.

When R_2 is **A** or **B** (Figure **2**), the desired enantiomers with the (3R, 4S) configurations had both more favorable enthalpic and entropic contributions, compared to the less potent enantiomers with the (3S, 4R) configurations, where enthalpy played a major role in the observed potent differences (compound **8-11** in Table **3**). No attempts were made to explain the observed thermodynamic signature differences of the enantiomers tested based on the x-ray crystal structures, although in theory it's plausible, for example, as reported in the case of enantiomers binding to acetylcholinesterase.[30] When R_2 is 7-fluoroindanyl **C**, we also observed favorable enthalpy change from compound **22** to **19** in Table **2.** Enthalpy again largely contributed to the observed potency difference, despite the unfavorable entropic change in this case. It seemed that small chemistry structure and stereochemistry changes could alter the observed thermodynamic signature significantly in these cases.

We discussed previously that the fast k_{on} and k_{off} rates of the EED HTS hits makes the hit selection based on kinetic signatures at the hit to lead stage less attractive. In the same manner, we also examined the thermodynamic signature of several of the EED HTS hits. It has been recommended that hits with more enthalpic contributions should be prioritized for further development. However, the challenges of doing this would be several-fold based on our studies. First, the potential requirement for analogs that are enantiomerically pure and of high purifies in order to get reliable K_D values from ITC experiments are much less feasible in the hit to lead stage where impurities may commonly present in the HTS hits and chirally pure compounds with high ee values may not be readily available for screening. This means that false negative results for hit confirmation will likely be common from ITC experiments. Secondly, slight

modifications to the chemical structure of the hits may cause significant change in the thermodynamic signature, thus making selection of a hit as a chemical series to work on less feasible. For example, by simply adding a dimethylamino group onto one of the HTS hits (compound **18** to **25**), we saw more than a four log unit change in both enthalpic and entropic contributions, with similar binding affinities however. The outcome of the prioritization of hits based on the thermodynamic signature would have been very different whether compound **18** or **25** was considered. Lastly, the lower throughput of ITC compared to other screening techniques such as TR-FRET assay and SPR binding measurement would make this technology less applicable for massive data collection in the hit-to-lead stage.

CONCLUSION. Undeniably, binding kinetics and thermodynamics are intrinsically connected with interactions between compounds and their protein targets. These interactions are essential for the function of all biomolecules, presumably also eventually the development of effective drugs with high efficacy and selectivity. The studies of the kinetic and thermodynamic signatures of compounds interacting with their protein targets in the context of the chemical structures have the potential to identify the structural features of the both the compound and the target protein that influence the formation and dissociation of the compound-protein complexes, which in turn aids the design of the compounds to maximize the compound-protein interaction.

In our study using the EED aminopyrrolidine series, the values of kinetic and thermodynamic parameters covered a broad range, making SKR and STR studies possible. As the program progressed, slower k_{off} rates were observed along with improved binding affinities. Both slower k_{off} rates and better binding affinity correlated with better cellular activities.

Our thermodynamic study of the EED chirally pure compounds showed that this series of compounds all exhibited favorable enthalpic contributions and unfavorable entropic contributions to binding affinity. The EED amino pyrrolidine series appeared to be largely enthalpy driven, which accounted for 60-80% of the observed binding affinity. As the program progressed, in general, we saw enthalpy- entropy compensation phenomenon. Moreover, in stark contrast to the view that ligands that have originated from medicinal chemistry optimization tend to display increased affinities due to enhancement in entropic contributions, we observed improved enthalpic contribution on our hit-to-lead EED program.

From our studies to incorporate thermodynamic and kinetic profiling on the EED hit-to-lead program, it became obvious that in order to evaluate the role of thermodynamic and kinetic data in the hit and lead optimization process, the first step would be to increase the throughput of the data generation. Biophysical technologies are now being increasingly applied to drug discovery processes. They are incorporated as part of an integral process in the HTS hit characterization and validation phase at many pharmaceutical companies.[31] For example, SPR is one of the most widely used biophysical techniques for obtaining binding affinities orthogonally, to confirm that compound of interest binds directly to the protein target of interest. However, significant challenges still exist however in getting SPR and ITC data routinely with acceptable cycle times comparable to the traditional biochemical assays, especially in the case of ITC. More than 800 EED amino pyrrolidine compounds were synthesized and profiled in the TR-FRET assay with fast turnaround times enabling rapid SAR iterations. However, less than 15% of these analogs were profiled in SPR and ITC, due to the longer testing cycles needed for data collection and processing, making the timely incorporation of this data in compound selection consideration much less feasible. This in turn, limited the practical use of kinetic and thermodynamic

information for prospective design, compared to other parameters that are easily obtainable. Significant instrumentation improvements have been seen in recent years. For example, biacore 8K can potentially characterize 64 interactions in 5 hours.

Our study also aimed to raise the awareness of the complexity of the ITC data interpretation. When compounds tested contain several stereoisomers, which have different binding affinities to the protein target tested, the apparent K_D determined from ITC experiments could be much higher than the K_D for the individual stereoisomer. In some cases, this difference could appear more than several thousand fold less potent. Most strikingly, we observed the presence of a small percentage of another stereoisomer could alter the apparent K_D dramatically and mask the true binding affinity of the compound of interest, which is not the case for TR-FRET and SPR measurements. Although in-depth study and more data are needed to elucidate the striking differences observed, we suspect the prevalence of such phenomenon, especially when using ITC for binding affinity determination in the early stage of the compound optimization process. Thus, ITC experiments must be interpreted in the context of chiral purities of the compounds.

Our study also demonstrated the difficulty in utilizing kinetic and thermodynamic information in hit selection and optimization. The prevalence of fast kinetics amongst the HTS hits made the compounds of interest kinetically indistinguishable. We have also suggested that the recommendation that a hit with more enthalpic binding affinity should be prioritized for hit optimization should be revisited. Clearly, small changes in structures can have profound changes in the enthalpic contribution.

We had attempted to interpret the observed SKR and STR based on high resolution X-ray crystal structures. The effects of polar groups and hydrogen bond acceptors/donors as mentioned

previsouly, as well as the positions of the various substituents and chirality in the context of the X-ray crystal structures were investigated. However, only limited speculations can be made due to the lack of the accurate information on compound-protein complex formation as well as available computational tools. For example, it should be noted that the observed ΔH and calculated -TΔS are global parameters, containing a mix of many contributions. It is widely acknowledged that the observed thermodynamic values reflect the sum of all coupled processes accompanying the binding process including such as solvation and desolvation stages of the compound, protein, and the complex formed. [32,33] These factors are not revealed by the static high resolution x-ray structures and may not be easily obtainable or identifiable. Our understanding of the multiple factors that influence compound-protein interactions is still rather rudimentary despite the enormous research efforts that went into the characterization of these factors. [34, 35] Similarly, a major challenge with optimization of the kinetic signature of a compound is the fundamental difficulty in characterizing transition states during the compound protein complex formation. Overall, the complexity of the compound-protein interactions and our limited knowledge in extricating the specific factors influencing kinetic and thermodynamic readouts at the macroscopic level means more research is warranted in these fields for their potential application in prospective design.

The dearth of the existing kinetic and especially thermodynamic data made the understanding of factors that govern the data readout particularly challenging. The limited datasets reported in the literature is evidently nowhere near the plethora of the available binding affinity data in literature.[22,34]

As such, it is our view that significant efforts are still needed to collect, analyze and understand kinetic and thermodynamic data.[36] Although both fields are still in their infancies with very few successful examples showing the essential role of thermodynamic and kinetic profiling in prospective design, the ultimate hope is that a multifaceted strategy will be developed to achieve a complete understanding of the interplay between all of these parameters to facilitate rational prospective molecule design in drug discovery.

EXPERIMENTAL SECTION

Descriptions of EED TR-FRET assay, cellular assay and X-ray crystallography have been reported previously.[17,19]

ITC experiment. ITC experiments were carried out on the Microcal Auto-ITC 200 system. The calorimeter has a sample cell volume of 200 ul and a syringe volume of 40 ul. However the fluidics system installed for automated sample handling requires a minimum of 370 ul for the cell and 120 ul for the syringe. A temperature controlled tray holding 96 well plates is integral to the instrument for storing samples; in this case at 10˚ C. Experiments were designed to enable the robotic arm to transfer both ligand and protein from the tray which was kept in the chamber at 10˚C. ITC runs were done at 25˚C using twenty 2 µl injections, each over 4 seconds with a delay of 3 minutes between injections. Data analysis was performed using the accompanying Origin software.

Protein preparation for the ITC experiments: Residues (77–441) of human EED were cloned into pET28b vector and expressed in Escherichia coli. BL21(DE3)-T1R strain. His-tagged protein was purified by Ni–Sepharose-6 affinity chromatography and finally on Superdex 200 column

(GE Healthcare) equilibrated with 20 mM Tris, 150 mM NaCl, 1 mM TCEP, pH 8.0. This buffer had been found optimal for EED long term stability from other studies and was also adopted for ITC, in spite of its large value for heat of ionization. Protein was defrosted from -80˚C and dialyzed against fresh column buffer overnight and concentrated next day on a 10,000 MWCO membrane centrifugal concentrator. Protein concentration was determined by absorbance at 280 nm. The majority of titrations were done in the reverse mode with 200 μM EED in the syringe, 20 μM ligand in the cell. Ligands were soluble at this concentration. To confirm, some titrations were also done with 20 μM protein in the cell and 200 μM ligand in the syringe, the forward mode. No attempt was made to artificially set the stoichiometry to 1.0 during curve fitting, and it was allowed to float during curve fitting with Origin.

SPR Binding Experiment. The binding kinetics of EED compounds were assayed via Surface Plasmon Resonance (SPR) using a Biacore T200 instrument (GE Healthcare and the software provided). Biotinylated EED (h)(78-441) was captured on neutravidin in flowcell 2. A blank surface had neutravidin saturated with biotin in flowcell 1 and used as a reference surface during binding assays. Briefly, the running buffer during neutravidin immobilization was HSB-P+ Buffer (10 mM Hepes, 150 mM NaCl, 0.05% (vol/vol) surfactant P20, pH 7.4) and the coupling procedure was run at a flow rate of 5uL/min. A neutravidin coupling solution was prepared by diluting neutavidin(Prod#31000 from Thermo Scientific) to 25 ug/mL in 10 mM acetate solution (pH 5.5). Carboxyl groups on the dextran layer of the chip were activated by injecting a 1:1 mixture of 0.4 M N-ethyl-N-(3dimethylaminopropyl)carbodiimide and 0.1 M N-hydroxysuccinimide for 7 min. The neutravidin coupling solution was injected over the activated chip surface for 300 sec at 10 ul/min to achieve a immobilization level of 14000 resonance units (RU). Remaining free activated carboxyl groups were blocked by injecting a

solution 1 M ethanolamine for 7 min. Binding affinities measurements were performed at flow rate of 100 uL/min using 20 mM Phos, pH 6.5, 150 mM NaCl, 0.05% Tween-20, containing 1 mM DTT and 3 % DMSO. Compounds were assayed using multi-cycle kinetics mode as provided by the Biacore T200 control software and were recorded at a frequency of 10 Hz. The compounds were diluted in the running buffer and injected in a series of increasing concentrations for contact time of 210 sec each and dissociation was monitored for up to 500 sec. Sensograms were processed and analyzed using Biacore T200 evaluation software, the binding curves were fit to determine the equilibrium dissociation constant (K_D).

Chemistry. Unless otherwise noted, all materials were obtained from commercial suppliers and used without further purification. Flash chromatography was performed using a Combi*flash*® Rf automated purification system. Preparative HPLC was performed on either an automated preparative-scale purification system equipped with a Waters Sunfire C8 5m column (150 x 30 mm) or on a Phenomenex Luna C8 5m 100Å AXIA column (50mm × 21.2mm). A gradient of acetonitrile (A) and 0.1% trifluoroacetic acid in water (B) was used, at a flow rate of 30 mL/min (0-0.5 min 5% A, 0.5-6.5 min linear gradient 5-100% A, 6.5-8.5 min 100% A, 8.5-9.0 min linear gradient 100-5% A, 9.0-10 min 5% A). Proton nuclear magnetic resonance spectra (^{1}H NMR, 500 or 400 MHz) were obtained in deuterodimethylsulfoxide (DMSO-d_6) with residual solvent as the internal standard unless otherwise noted. Mass spectra (MS) were obtained by ionizing samples via positive electron spray ionization (ESI) or desorption chemical ionization (DCI) with TOF as the mass analyzer. Preparative chiral SFC was performed on a THAR/Waters SFC 80 system running under SuperChrom software control. The sample was dissolved in a 8:1:1 mixture of methanol/dichloromethane/dimethylsulfoxide at a concentration of 15 mg/mL. The sample was loaded into the modifier stream in 1 mL (15 mg) injections. The

mobile phase was held isocratically at 30% methanol:CO_2. The instrument was fitted with a Chiralpak IA column with dimensions 21 mm i.d. x 250 mm length with 5 μm particles. Chiral purities were determined by chiral SFC columns. All compounds described and characterized herein are of ≥95% purity as assessed by ^{1}H NMR and LC-MS.

Detailed synthesis and characterization data of compounds **1-2** and **23-24** has been reported.[17,19] Other compounds **3-16** and **19-22** follow the similar synthetic routes as described for compound **2**.

1-(4-(4-(4-(dimethylamino)-1-(2-fluoro-6-methylbenzyl)pyrrolidin-3-yl)phenyl)piperazin-1-yl)ethanone (3). *Step 1.* A mixture of 1-benzyl-4-(4-bromophenyl)pyrrolidin-3-amine (55 g, 166 mmol)17 and di-*tert*-butyl dicarbonate (73 g, 332 mmol) were stirred in a round bottom flask in 500 ml ethanol at room temperature overnight. The reaction mixture was concentrated and purified by flash chromatography to give 35g *tert*-butyl (1-benzyl-4-(4-bromophenyl)pyrrolidin-3-yl)carbamate with 50% isolated yield.

Step 2. To a solution of *tert*-butyl (1-benzyl-4-(4-bromophenyl)pyrrolidin-3-yl)carbamate from step 1 (5 g, 11.6 mmol) in dichloroethane 60 ml was added triethylamine (7.0 g, 69.5 mmol) followed by 1-chloroethyl carbonochloridate (9.9 g, 69.5 mmol). The mixture was stirred at 80 °C overnight and extracted by dichloromethane followed by saturated NH_4Cl solution. The combined organic phases were dried over Na_2SO_4 and concentrated to give the crude material as brown oil. This crude material was refluxed in 60 ml MeOH for 2 hr, concentrated and partitioned between dichloromethane and pH = 1 HCl aqueous solution. After separation, the aqueous phase was basified to pH = 9 with sodium bicarbonate and extracted with

dichloromethane to give *tert*-butyl (4-(4-bromophenyl)pyrrolidin-3-yl)carbamate(1.32 g, 3.9 mmol) with 33% yield after purification.

Step 3. To *tert*-butyl (4-(4-bromophenyl)pyrrolidin-3-yl)carbamate (800 mg, 2.3 mmol) from step 2 in pH = 4 buffer solution in MeOH, sodium cyanoborohydride (221 mg, 3.52 mmol) and 2-fluoro-6-methylbenzaldehyde (356 mg, 2.58 mmol) were added and stirred at room temperature for 2 hr. The reaction mixture was partitioned between water and dichloromethane. The organic layer was concentrated and purified via flash chromatography to give *tert*-butyl 4-(4-bromophenyl)-1-(2-fluoro-6-methylbenzyl)pyrrolidin-3-yl)carbamate as a white solid (870 mg, 1.88 mmol) with 80% isolated yield.

Step 4. To *tert*-butyl 4-(4-bromophenyl)-1-(2-fluoro-6-methylbenzyl)pyrrolidin-3-yl)carbamate obtained from step 3 (870 mg, 1.88 mmol) was added 4 ml dioxane and 3 ml 4N HCl in dioxane. The mixture was stirred at room temperature for 2 hr and then concentrated down to afford 4-(4-bromophenyl)-1-(2-fluoro-6-methylbenzyl)pyrrolidin-3-amine as HCl salt with quantitative yield. To this material, 8 ml pH=4 buffer in MeOH, formaldehyde (0.7 ml, 9.3 mmol) and sodium cyanoborohydride (176 mg, 2.8 mmol) were then added. The reaction mixture was stirred at room temperature for 3 hr then partitioned between dichloromethane and saturated sodium bicarbonate solution. The organic layer was separated, dried and concentrated down to give 4-(4-bromophenyl)-1-(2-fluoro-6-methylbenzyl)-N,N-dimethylpyrrolidin-3-amine, which was used in the next step without further purification.

Step 5. A microwave vial was charged with 4-(4-bromophenyl)-1-(2-fluoro-6-methylbenzyl)-N,N-dimethylpyrrolidin-3-amine (60 mg, 0.15 mmol), $Pd_2(dba)_3$ (14 mg, 0.015mmol), 2-(dicyclohexylphosphine)-2',4',6'-tri-isopropylbiphenyl (14.6 mg, 0.031 mmol) and sodium tert-

butoxide (22 mg, 0.23 mmol) under nitrogen in 0.6 ml dioxane. This mixture was heated at 110 °C for 0.5 hr and then diluted with ethyl acetate followed by filtration through a pad of celite. The filtrate was concentrated and dissolved in 1.5 ml DMSO/MeOH (1:1). Preparative HPLC purification afforded compound **3** as TFA salts with 78% isolated yield. ^{1}H NMR (500 MHz, DMSO-d6) δ 7.30 (m, 2H), 7.12 – 7.00 (m, 3H), 6.95 (d, J = 8.8 Hz, 2H), 3.74-4.0 (m, 4H), 3.57 (m, 6H), 3.11 (m, 5H), 2.71 (s, 6H), 2.70 (m, 1H), 2.43 (s, 3H), 2.04 (s, 3H). MS (ESI) m/z = 439 $(M+H)^+$.

1-(4-(4-((-(dimethylamino)-1-(7-fluoro-2,3-dihydro-1H-inden-1-yl)pyrrolidin-3-yl)phenyl)piperazin-1-yl)ethanone (4). Compound **4** was synthesized using the similar synthetic route as for compound **3**, substituting 7-fluoro-2,3-dihydro-1H-inden-1-one for 2-fluoro-6-methylbenzaldehyde. The compound was an approx. 67:33 mixture of epimers as assessed by ^{1}H NMR: ^{1}H NMR (400 MHz, DMSO-*d*6) δ 7.31 –7.21 (m, 1H), 7.16 (dd, J = 8.8, 2.3 Hz, 2H), 7.09 (d, J = 7.4 Hz, 1H), 6.95 (td, J = 8.8, 5.2 Hz, 1H), 6.86 (dd, J= 8.7, 3.3 Hz, 2H), 4.18 (dd, J = 7.0, 1.7 Hz, 0.33H), 4.19 (dd, J = 6.9, 1.7 Hz, 0.67H), 3.61-3.50 (m, 4H), 3.15 – 2.92 (m, 6H), 2.89-2.73 (m, 4H), 2.65-2.52 (m, 1H), 2.48 – 2.35 (m, 1H), 2.34 – 2.11 (m, 1H), 2.14 – 1.93 (m, 7H), 1.88 (s, 3H). MS (ESI) *m/z* 451 $(M+H)^+$.

1-(2-bromo-6-fluorobenzyl)-4-(3,4-dimethoxyphenyl)-N,N-dimethylpyrrolidin-3-amine (5). *Step 1*. To a solution of (*E*)-1,2-dimethoxy-4-(2-nitrovinyl)benzene (40 g, 191 mmol) in dichloromethane 500 ml was added N-benzyl-1-methoxy-N-((trimethylsilyl)methyl)methanamine (54.5 g, 229 mmol). The resulting solution was cooled to -10 ^{o}C using salt-ice bath and then TFA (1.473 mL, 19.12 mmol) was added dropwise (Caution: severely exothermic). After addition, the reaction was stirred at -10 ^{o}C for 1 hour, and then allowed to warm to room temperature and stirred at this temperature for 16 hr. The contents were

then poured into saturated sodium bicarbonate solution. The organic layer was separated, washed with water and brine respectively, and then concentrated under reduced pressure. The residue was purified by flash column chromatography to afford 1-benzyl-3-(3,4-dimethoxyphenyl)-4-nitropyrrolidine (35 g, 102 mmol)as a yellow oil with 54% yield.

Step 2. To a solution of 1-benzyl-3-(3,4-dimethoxyphenyl)-4-nitropyrrolidine (60 g, 175 mmol) in EtOH 2000 ml was added Raney Ni 20g. The mixture was stirred under H_2 and 15 psi at 25 °C for 2 hr. The mixture was filtered and concentrated to give 1-benzyl-4-(3,4-dimethoxyphenyl)pyrrolidin-3-amine as a yellow oil. The crude material was dissolved in 500 ml EtOH. To this, Boc_2O (53.5 mL, 230 mmol) was added and stirred at 25 °C for 12 hr, The mixture was concentrated down to give *tert*-butyl (1-benzyl-4-(3,4-dimethoxyphenyl)pyrrolidin-3-yl)carbamate (20 g, 48.5 mmol) as a white solid with a 25% yield.

Step 3. a suspension of *tert*-butyl (-1-benzyl-4-(3,4-dimethoxyphenyl)pyrrolidin-3-yl)carbamate (20 g, 48.5 mmol) and Pd/C (5 g) in MeOH 1000 ml was stirred at 25 °C for 24 hr under Hydrogen (15 psi). After filtration and solvent removal, The crude product was recrystallized to give *tert*-butyl (4-(3,4-dimethoxyphenyl)pyrrolidin-3-yl)carbamate (13.5 g, 41.9 mmol) as white solid with 86% yield.

Step 4. To a solution of *tert*-butyl (4-(3,4-dimethoxyphenyl)pyrrolidin-3-yl)carbamate (35 mg, 0.11mmol) in 1 mL pH=4 buffer solution in MeOH, 2-bromo-6-fluorobenzaldehyde (33 mg, 0.16 mmol) and sodium cyanoborohydride (6.4 mg, 0.16 mmol) were added. The mixture was stirred at room temperature for 4 hr. The reaction mixture is partitioned between dichloromethane and saturated sodium bicarbonate solution. The organic layer was separated, dried and concentrated down. To the crude material thus obtained, 1 ml dioxane and 0.5 ml 4 N

HCl in dioxane were added. After 2 hr at room temperature, the mixture was dried down and 1 ml pH=4 buffer in MeOH, formaldehyde (0.04 ml, 0.55 mmol) and sodium cyanoborohydride (6.4 mg, 0.16 mmol) were added. The reaction mixture was stirred at room temperature for 3 hr, then partitioned between dichloromethane and saturated sodium bicarbonate solution. The organic layer was separated, dried and concentrated down. The crude material was purified by reverse phase HPLC to give 11 mg of 1-(2-bromo-6-fluorobenzyl)-4-(3,4-dimethoxyphenyl)-N,N-dimethylpyrrolidin-3-amine as a TFA salt with 11% overall yield. ^{1}H NMR (500 MHz, Pyridine-d_5) δ 7.48 – 7.42 (m, 1H), 7.19 – 7.06 (m, 3H), 7.01 (dd, J = 8.2, 2.1 Hz, 1H), 6.92 (d, J = 8.3 Hz, 1H), 3.91 (q, J = 6.1 Hz, 1H), 3.81 – 3.66 (m, 9H), 3.28 – 3.18 (m, 3H), 2.78 (s, 6H), 2.70 (dd, J = 9.1, 5.7 Hz, 1H). MS (ESI) *m/z* 439 $(M+H)^+$.

4-(3,4-dimethoxyphenyl)-1-(2-fluoro-6-methylbenzyl)-N,N-dimethylpyrrolidin-3-amine (6). Compound **6** was synthesized using the similar synthetic route as for compound **5**, substituting 2-fluoro-6-methylbenzaldehyde for 2-fluoro-6-bromobenzaldehyde. ^{1}H NMR (500 MHz, Pyridine-d_5) δ 7.21 – 7.15 (m, 1H), 7.13 (d, J = 2.1 Hz, 1H), 7.04 – 6.96 (m, 3H), 6.92 (d, J = 8.3 Hz, 1H), 3.96 (dt, J = 7.6, 5.1 Hz, 1H), 3.77 (m, 7H), 3.68 – 3.60 (m, 2H), 3.29 – 3.12 (m, 3H), 2.79 (s, 6H), 2.62 (dd, J = 9.1, 6.2 Hz, 1H), 2.41 (s, 3H). MS (ESI) *m/z* 373 $(M+H)^+$.

4-(3,4-dimethoxyphenyl)-1-(7-fluoro-2,3-dihydro-1H-inden-1-yl)-N,N-dimethylpyrrolidin-3-amine (7). Compound **7** was synthesized using the similar synthetic route as for compound **5**, substituting 7-fluoro-2,3-dihydro-1H-inden-1-one for 2-fluoro-6-bromobenzaldehyde. The compound was an approx. 66:34 mixture of epimers as assessed by ^{1}H NMR: ^{1}H NMR (400 MHz, DMSO-d_6) δ 7.26 (tdd, J = 7.6, 5.2, 2.1 Hz, 1H), 7.10 (d, J = 7.3 Hz, 1H), 6.96 (dd, J = 12.4, 5.5 Hz, 2H), 6.80 (d, J = 3.1 Hz, 2H), 4.25 (m, 1H), 3.73 – 3.67 (m, 6H), 3.10 – 2.95 (m,

2H), 2.95 – 2.74 (m, 4H), 2.69 – 2.51 (m, 1H), 2.50 – 2.39 (m, 1H), 2.32 – 2.14 (m, 1H), 2.14 – 1.93 (m, 7H). MS (ESI) *m/z* 385 $(M+H)^+$.

(3S,4R)-1-(2-bromo-6-fluorobenzyl)-N,N-dimethyl-4-(1-methyl-1H-indol-3-yl)pyrrolidin-3-amine (8). The racemic compound 1-(2-bromo-6-fluorobenzyl)-N,N-dimethyl-4-(1-methyl-1H-indol-3-yl)pyrrolidin-3-amine (compound **15**) was synthesized using the similar synthetic route as for compound **5**, substituting (*E*)-3-(2-nitrovinyl)-1H-indole for (*E*)-1,2-dimethoxy-4-(2-nitrovinyl)benzene. The racemic material (594 mg of compound **15**) was chirally separated on a Chiralpak column (retention time = 6.7 min) to give 215 mg (3S,4R)-1-(2-bromo-6-fluorobenzyl)-N,N-dimethyl-4-(1-methyl-1H-indol-3-yl)pyrrolidin-3-amine (ee = 100%). ^{1}H NMR (400 MHz, Chloroform-*d*) δ 7.91 (dt, *J* = 8.0, 1.0 Hz, 1H), 7.41 (dt, *J* = 8.0, 1.1 Hz, 1H), 7.32 – 7.20 (m, 2H), 7.16 – 7.07 (m, 2H), 7.02 (ddd, *J* = 9.5, 8.3, 1.2 Hz, 1H), 6.97 (s, 1H), 3.88 (d, *J* = 2.7 Hz, 2H), 3.74 (s, 3H), 3.48 (dt, *J* = 8.4, 5.0 Hz, 1H), 3.19 – 3.02 (m, 3H), 2.86 – 2.67 (m, 2H), 2.24 (s, 6H). MS (ESI) *m/z* 432 $(M+H)^+$.

(3R,4S)-1-(2-bromo-6-fluorobenzyl)-N,N-dimethyl-4-(1-methyl-1H-indol-3-yl)pyrrolidin-3-amine (9). The racemic compound 1-(2-bromo-6-fluorobenzyl)-N,N-dimethyl-4-(1-methyl-1H-indol-3-yl)pyrrolidin-3-amine (compound **15**) was synthesized using the similar synthetic route as for compound **5**, substituting (*E*)-3-(2-nitrovinyl)-1H-indole for (*E*)-1,2-dimethoxy-4-(2-nitrovinyl)benzene. The racemic material (594 mg) was chirally separated on a Chiralpak column (retention time = 7.5 min) to give 226 mg (3R,4S)-1-(2-bromo-6-fluorobenzyl)-N,N-dimethyl-4-(1-methyl-1H-indol-3-yl)pyrrolidin-3-amine (ee = 99%). ^{1}H NMR (400 MHz, Chloroform-*d*) δ 7.91 (dt, *J* = 8.0, 1.0 Hz, 1H), 7.41 (dt, *J* = 8.0, 1.1 Hz, 1H), 7.32 – 7.20 (m, 2H), 7.16 – 7.07 (m, 2H), 7.02 (ddd, *J* = 9.5, 8.3, 1.2 Hz, 1H), 6.97 (s, 1H), 3.88 (d, *J* = 2.7 Hz,

2H), 3.74 (s, 3H), 3.48 (dt, *J* = 8.4, 5.0 Hz, 1H), 3.19 – 3.02 (m, 3H), 2.86 – 2.67 (m, 2H), 2.24 (s, 6H). MS (ESI) *m/z* 432 $(M+H)^+$.

(3S,4R)-1-(2-fluoro-6-methylbenzyl)-N,N-dimethyl-4-(4-(methylsulfonyl)phenyl)pyrrolidin-3-amine (10). The racemic compound 1-(2-fluoro-6-methylbenzyl)-N,N-dimethyl-4-(4-(methylsulfonyl)phenyl)pyrrolidin-3-amine was synthesized using the similar synthetic route as for compound **5**, substituting (*E*)-1-(methylsulfonyl)-4-(2-nitrovinyl)benzene for (*E*)-1,2-dimethoxy-4-(2-nitrovinyl)benzene and 2-fluoro-6-methylbenzaldehyde for 2-bromo-6-fluorobenzaldehyde. The racemic material (70 mg) was chirally separated on a RegisPack 250mm column (retention time = 2.9 min) to give 20 mg (3S,4R)-1-(2-fluoro-6-methylbenzyl)-N,N-dimethyl-4-(4-(methylsulfonyl)phenyl)pyrrolidin-3-amine (ee = 100%). ^{1}H NMR (400 MHz, Methanol-d_4) δ 7.99 – 7.85 (m, 2H), 7.74 – 7.60 (m, 2H), 7.21 (td, *J* = 7.9, 5.8 Hz, 1H), 7.04 (d, *J* = 7.6 Hz, 1H), 6.92 (t, *J* = 9.1 Hz, 1H), 4.14 – 3.96 (m, 1H), 3.71 (q, *J* = 7.4 Hz, 1H), 3.20 (m, 5H), 3.11 (s, 3H), 2.82 (s, 6H), 2.61 (t, *J* = 8.5 Hz, 1H), 2.46 (s, 3H). MS (ESI) *m/z* 392 $(M+H)^+$.

(3R,4S)-1-(2-fluoro-6-methylbenzyl)-N,N-dimethyl-4-(4-(methylsulfonyl)phenyl)pyrrolidin-3-amine (11). The racemic compound 1-(2-fluoro-6-methylbenzyl)-N,N-dimethyl-4-(4-(methylsulfonyl)phenyl)pyrrolidin-3-amine was synthesized using the similar synthetic route as for compound **5**, substituting (*E*)-1-(methylsulfonyl)-4-(2-nitrovinyl)benzene for (*E*)-1,2-dimethoxy-4-(2-nitrovinyl)benzene and 2-fluoro-6-methylbenzaldehyde for 2-bromo-6-fluorobenzaldehyde. The racemic material (70 mg) was chirally separated on a RegisPack 250mm column (retention time = 4.6 min) to give 25 mg (3R,4S)-1-(2-fluoro-6-methylbenzyl)-N,N-dimethyl-4-(4-(methylsulfonyl)phenyl)pyrrolidin-3-

amine (ee = 100%). ^{1}H NMR (400 MHz, Methanol-d_4) δ 7.99 – 7.85 (m, 2H), 7.74 – 7.60 (m, 2H), 7.21 (td, *J* = 7.9, 5.8 Hz, 1H), 7.04 (d, *J* = 7.6 Hz, 1H), 6.92 (t, *J* = 9.1 Hz, 1H), 4.14 – 3.96 (m, 1H), 3.71 (q, *J* = 7.4 Hz, 1H), 3.20 (m, 5H), 3.11 (s, 3H), 2.82 (s, 6H), 2.61 (t, *J* = 8.5 Hz, 1H), 2.46 (s, 3H). MS (ESI) *m/z* 392 $(M+H)^+$.

1-(2-bromo-6-fluorobenzyl)-N,N-dimethyl-4-phenylpyrrolidin-3-amine (12). Compound **12** was synthesized using the similar synthetic route as for compound **5**, substituting (*E*)-(2-nitrovinyl)benzene for (*E*)-1,2-dimethoxy-4-(2-nitrovinyl)benzene. ^{1}H NMR (500 MHz, Pyridine-d_5) δ 7.48 – 7.39 (m, 3H), 7.36 (t, *J* = 7.5 Hz, 2H), 7.27 (t, *J* = 7.3 Hz, 1H), 7.22 (m, 1H), 7.18 – 7.02 (m, 2H), 3.88 – 3.63 (m, 4H), 3.31 (dd, *J* = 10.3, 4.5 Hz, 1H), 3.24 – 3.05 (m, 2H), 2.68 (s, 6H), 2.59 (dd, *J* = 9.1, 6.6 Hz, 1H). MS (ESI) *m/z* 377 $(M+H)^+$.

4-(1-(2-bromo-6-fluorobenzyl)-4-(dimethylamino)pyrrolidin-3-yl)phenol (13). Compound **13** was synthesized using the similar synthetic route as for compound **5**, substituting (*E*)-4-(2-nitrovinyl) phenol for (*E*)-1,2-dimethoxy-4-(2-nitrovinyl)benzene. ^{1}H NMR (501 MHz, DMSO-d_6) δ 7.53 (d, *J* = 7.9 Hz, 1H), 7.37 – 7.24 (m, 2H), 7.24 – 7.16 (m, 2H), 6.75 – 6.66 (m, 2H), 3.92 – 3.71 (m, 3H), 3.45 (td, *J* = 7.8, 5.2 Hz, 2H), 3.18 – 3.04 (m, 2H), 2.71 (s, 6H), 2.44 (m, 1H). MS (ESI) *m/z* 393 $(M+H)^+$.

4-(1-(2-bromo-6-fluorobenzyl)-4-(dimethylamino)pyrrolidin-3-yl)phenol (14). Compound **14** was synthesized using the similar synthetic route as for compound **5**, substituting (*E*)-2-(2-nitrovinyl)pyridine for (*E*)-1,2-dimethoxy-4-(2-nitrovinyl)benzene. ^{1}H NMR (500 MHz, DMSO-d_6) δ 7.77 (tt, *J* = 7.7, 2.3 Hz, 1H), 7.53 (tt, *J* = 7.6, 1.0 Hz, 1H), 7.47 – 7.21 (m, 5H), 4.32 – 4.22 (m, 1H), 3.87 – 3.70 (m, 3H), 3.28 – 3.18 (m, 2H), 2.95 – 2.84 (m, 1H), 2.72 (s, 6H), 2.43 (t, *J* = 8.5 Hz, 1H). MS (ESI) *m/z* 378 $(M+H)^+$.

3-bromo-4-((3-(dimethylamino)-4-(1-methyl-1H-indol-3-yl)pyrrolidin-1-yl)methyl)-5-fluorophenol (16). N,N-dimethyl-4-(1-methyl-1H-indol-3-yl)pyrrolidin-3-amine[17] (50mg, 0.21 mmol) and 2-bromo-6-fluoro-4-hydroxybenzaldehyde (47.2 mg, 0.22mmol) in pH=4 buffer MeOH solution was added MP-BH_3CN (196 mg, 0.411 mmol, 2.1 mmol/g). The mixture was shaken at room temperature overnight then filtered, dried down and purified on reverse phase HPLC to give 68.5 mg product as a TFA salt with 49% yield. ^{1}H NMR (400 MHz, DMSO-d_6) δ 7.74 (d, J = 7.9 Hz, 1H), 7.42 (t, J = 4.1 Hz, 2H), 7.18 (t, J = 7.6 Hz, 1H), 7.05 (t, J = 7.5 Hz, 1H), 6.95 (t, J = 1.6 Hz, 1H), 6.67 (dd, J = 11.6, 2.4 Hz, 1H), 4.14 (dd, J = 13.9, 7.9 Hz, 1H), 4.03 – 3.81 (m, 3H), 3.74 (s, 3H), 3.36 (m 3H), 2.76 (s, 6H), 2.78 (m, 1H). MS (ESI) *m/z* 446 $(M+H)^+$.

(4-(2-methoxyphenyl)piperazin-1-yl)(2-(methylsulfonyl)phenyl)methanone (17). (4-(2-methoxyphenyl)piperazin-1-yl)(2-(methylthio)phenyl)methanone (140 mg, 0.81 mmol) in 2 ml dichloromethane was added m-CPBA (140mg, 0.81mmol). The reaction mixture was stirred overnight and quenched with aqueous $Na_2S_2O_5$ solution followed by extraction with ethyl acetate. The organic layer was dried down and purified via flash chromatography to give 38 mg product with 35% yield. ^{1}H NMR (400 MHz, DMSO-d_6) δ 7.99 (dd, J = 7.9, 1.2 Hz, 1H), 7.81 (td, J = 7.5, 1.3 Hz, 1H), 7.71 (td, J = 7.7, 1.3 Hz, 1H), 7.54 (dd, J = 7.6, 1.3 Hz, 1H), 7.03 – 6.83 (m, 4H), 3.77 (s, 3H), 3.76 (m, 2H), 3.28 (s, 3H), 3.29 (m, 1H), 3.19 (ddd, J = 13.0, 6.3, 3.5 Hz, 1H), 3.04 (q, J = 4.4, 3.3 Hz, 2H), 2.92 (dq, J = 9.4, 6.7, 5.7 Hz, 2H). MS (ESI) *m/z* 375 $(M+H)^+$.

4-(3,4-dihydroisoquinolin-2(1H)-yl)-N,N-dimethylpyridin-2-amine (18). 1,2,3,4-tetrahydroisoquinoline (400 mg, 3.0 mmol) and 4-chloropyridine hydrochloride (451mg, 3.0 mmol) in 3 ml NMP were added triethyl amine (1.0 ml, 7.5 mmol). The reaction mixture was heated to 150°C for 2 hr. After cooling down, ethyl acetate was added and the mixture was

washed with water. The organic layer was separated and dried down. After flash chromatography, 200 mg of the product was obtained with 32% yield. ^{1}H NMR (400 MHz, DMSO-d_6) δ 8.37 – 7.92 (m, 2H), 7.42 – 7.02 (m, 4H), 7.00 – 6.62 (m, 2H), 4.50 (s, 2H), 3.60 (t, J = 6.0 Hz, 2H), 2.91 (t, J = 5.9 Hz, 2H). MS (ESI) *m/z* 211 $(M+H)^+$.

1-(4-(4-((3S,4R)-4-(dimethylamino)-1-((S)-7-fluoro-2,3-dihydro-1H-inden-1-yl)pyrrolidin-3-yl)phenyl)piperazin-1-yl)ethanone (19). 230 mg of Compound **4** was separated by chiral column to give 44 mg of compound **19** (retention time = 4.5 min, ee =100%). ^{1}H NMR (400 MHz, DMSO-d_6) δ 7.25 (td, J = 7.8, 5.2 Hz, 1H), 7.20 – 7.13 (m, 2H), 7.10 (d, J = 7.4 Hz, 1H), 6.95 (t, J = 8.8 Hz, 1H), 6.90 – 6.80 (m, 2H), 4.18 (dd, J = 6.8, 1.7 Hz, 1H), 3.55 (dt, J = 6.8, 3.9 Hz, 4H), 3.15 – 2.92 (m, 6H), 2.90 – 2.72 (m, 4H), 2.65 (dd, J = 8.8, 5.6 Hz, 1H), 2.43 (t, J = 7.7 Hz, 1H), 2.20 (ddt, J = 11.8, 7.6, 2.1 Hz, 1H), 2.04 (d, J = 6.5 Hz, 10H).MS (ESI) *m/z* 451 $(M+H)^+$.

1-(4-(4-((3S,4R)-4-(dimethylamino)-1-((R)-7-fluoro-2,3-dihydro-1H-inden-1-yl)pyrrolidin-3-yl)phenyl)piperazin-1-yl)ethanone (compound 20). 230 mg of Compound 4 was separated by chiral column to give 16 mg of compound **20** (retention time = 5.0 min, ee = 90%). ^{1}H NMR (400 MHz, DMSO-d_6) δ ^{1}H NMR (400 MHz, DMSO-d_6) δ δ 7.26 (td, J = 7.8, 5.2 Hz, 1H), 7.21 – 7.13 (m, 2H), 7.10 (d, J = 7.3 Hz, 1H), 6.96 (t, J = 8.8 Hz, 1H), 6.90 – 6.76 (m, 2H), 4.34 (dd, J = 7.3, 1.8 Hz, 1H), 3.54 (dt, J = 6.8, 3.7 Hz, 4H), 3.14 – 2.92 (m, 6H), 2.91 – 2.69 (m, 4H), 2.57 – 2.52 (m, 1H), 2.41 (dd, J = 8.7, 6.2 Hz, 1H), 2.18 (ddt, J = 12.2, 7.7, 2.3 Hz, 1H), 2.12 – 1.98 (m, 10H).. MS (ESI) *m/z* 451 $(M+H)^+$.

1-(4-(4-((3R,4S)-4-(dimethylamino)-1-((S)-7-fluoro-2,3-dihydro-1H-inden-1-yl)pyrrolidin-3-yl)phenyl)piperazin-1-yl)ethanone (compound 21). 230 mg of Compound 4 was separated

by chiral column to give 27 mg of compound **21** (retention time = 5.8 min , ee = 90%). ^{1}H NMR (400 MHz, DMSO-d_6) δ 7.25 (td, J = 7.8, 5.2 Hz, 1H), 7.20 – 7.13 (m, 2H), 7.10 (d, J = 7.4 Hz, 1H), 6.95 (t, J = 8.8 Hz, 1H), 6.90 – 6.80 (m, 2H), 4.18 (dd, J = 6.8, 1.7 Hz, 1H), 3.55 (dt, J = 6.8, 3.9 Hz, 4H), 3.15 – 2.92 (m, 6H), 2.90 – 2.72 (m, 4H), 2.65 (dd, J = 8.8, 5.6 Hz, 1H), 2.43 (t, J = 7.7 Hz, 1H), 2.20 (ddt, J = 11.8, 7.6, 2.1 Hz, 1H), 2.04 (d, J = 6.5 Hz, 10H).MS (ESI) *m/z* 451 $(M+H)^+$.

1-(4-(4-((3R,4S)-4-(dimethylamino)-1-((R)-7-fluoro-2,3-dihydro-1H-inden-1-yl)pyrrolidin-3-yl)phenyl)piperazin-1-yl)ethanone (compound 22). 230 mg of Compound 4 was separated by chiral column to give 24 mg of compound **22** (retention time = 6.7 min, ee = 100%). ^{1}H NMR (400 MHz, DMSO-d_6) δ ^{1}H NMR (400 MHz, DMSO-d_6) δ ^{1}H NMR (400 MHz, DMSO-d_6) δ 7.26 (td, J = 7.8, 5.2 Hz, 1H), 7.21 – 7.13 (m, 2H), 7.10 (d, J = 7.3 Hz, 1H), 6.96 (t, J = 8.8 Hz, 1H), 6.90 – 6.76 (m, 2H), 4.34 (dd, J = 7.3, 1.8 Hz, 1H), 3.54 (dt, J = 6.8, 3.7 Hz, 4H), 3.14 – 2.92 (m, 6H), 2.91 – 2.69 (m, 4H), 2.57 – 2.52 (m, 1H), 2.41 (dd, J = 8.7, 6.2 Hz, 1H), 2.18 (ddt, J = 12.2, 7.7, 2.3 Hz, 1H), 2.12 – 1.98 (m, 10H). MS (ESI) *m/z* 451 $(M+H)^+$.

4-(3,4-dihydroisoquinolin-2(1H)-yl)-N,N-dimethylpyridin-2-amine (25). 4-(3,4-dihydroisoquinolin-2(1H)-yl)pyridin-2-amine (100 mg, 0.44 mmol) in 1 ml pH=4 MeOH solution was added 0.1 ml 37% formaldehyde followed by sodium cyanoborohydride (30 mg, 0.48 mmol). The mixture was shaken at room temperature for 2 days at which time another 0.1 ml of 37% formaldehyde and 30 mg sodium cyanoborohydride were added. The mixture was shaken for additional 3 days. After reverse phase HPLC purification, 28 mg of the product was isolated with 25% yield. ^{1}H NMR (400 MHz, DMSO-d_6) δ 7.73 – 7.57 (m, 1H), 7.43 – 7.07 (m, 4H), 6.70 (dd, J = 7.6, 2.4 Hz, 1H), 5.96 (d, J = 2.4 Hz, 1H), 4.70 (s, 2H), 3.75 (t, J = 6.0 Hz, 2H), 3.14 (s, 6H), 2.96 (t, J = 6.0 Hz, 2H). MS (ESI) *m/z* 254 $(M+H)^+$.

AUTHOR INFORMATION

Corresponding Author

*Phone: +1 847-935-3058; E-mail: wang.ying@abbvie.com

ACKNOWLEDGMENT

All authors are employees of AbbVie. This study was sponsored by AbbVie. AbbVie contributed to the study design, research, and interpretation of data, writing, reviewing, and approving the manuscript. The authors wish to thank the EED chemistry team, oncology early discovery, high-throughput chemistry group, analytical purification sciences group, structural chemistry group, structural biology team and molecular modeling team. The authors also wish to thank Haizhong Zhu for EED biacore protein synthesis and many AbbVie medicinal chemists for helpful discussions.

ABBREVIATIONS

SAR, Structural-activity relationships; SKR, structural-kinetics relationships; STR, structural-thermodynamics relationships; ITC, isothermal titration calorimetry; SPR, surface plasmon resonance; EED, embryonic ectoderm development; HTS, high throughput screening; EZH2, enhancer of zester homolog 2; PRC2, polycomb repressive complex 2; TSA, thermal shift assay; ee, enantiomeric excess. TFA, trifluoroacetic acid.

SUPPORTING INFORMATION

Reaction scheme for the synthesis of compound 3, 5 and 16, binding curves from biacore and TR-FRET experiments, and ITC data output, molecular formula strings (CSV)

REFERENCES

(1) Lipinski, C. A.; Lombardo, F.; Dominy, B. W.; Feeney, P. J. Experimental and computational approaches to estimate solubility and permeability in drug discovery and development settings. *Adv. Drug Deliv. Rev.* **1997,** *23,* 3-25.

(2) Swinney D, C. The role of binding kinetics in therapeutically useful drug action. *Curr. Opin. Drug Discov. Devel.* **2009**, *1,* 31-39.

(3) Copeland, R, A. The dynamics of drug-target interactions: drug-target residence time and its impact on efficacy and safety. *Expert Opin. Drug Discov.* **2010,** *4,* 305-310.

(4) Ernesto, F. Do enthalpy and entropy distinguish first in class from best in class? *Drug Discov. Today* **2008,** *13,* 869-874.

(5) Ladbury, J. E.; Klebe, G.; Freire, E. Adding calorimetric data to decision making in lead discovery: a hot tip. *Nat. Rev. Drug Discov.* **2010,** *9,* 23-27.

(6) Copeland, R. A.; Pompliano, D. L.; Meek, T. D. Drug–target residence time and its implications for lead optimization. *Nat. Rev. Drug Discov.* **2006,** *5,* 730-739.

(7) Lu, H.; Tonge, P. J. Drug-target residence time: critical information for lead optimization. *Curr. Opin. Chem. Biol.* **2010,** *4,* 467-474.

(8) Guo, D.; Hillger, J. M.; IJzerman, A. P.; Heitman, L. H. Drug-target residence time—A case for G protein-coupled receptors. *Med. Res. Rev.* **2014,** *0,* 1-37.

(9) Vilums, M.; Zweemer, A. J. M.; Yu, Z.; Vries, H.; Hillger, J. M.; Wapenaar, H.; Bollen, I. A.; Barmare, F.; Gross, R.; Clemens, J.; Krenitsky, P.; Brussee, J.; Stamos, D.; Saunders, J.; Heitman, L. H.; IJzerman, A. P. Structure–kinetic relationships—an overlooked parameter in hit-to-lead optimization: a case of cyclopentylamines as chemokine receptor 2 antagonists. *J. Med. Chem.* **2013,** *56,* 7706–7714.

(10) Ladbury, J. E. Calorimetry as a tool for understanding biomolecular interactions and an aid to drug design. *Biochem. Soc. Trans.* **2010,** *38,* 888-893.

(11) Biela , A.; Sielaff , F.; Terwesten, F.; Heine, A.; Steinmetzer, T.; Klebe, G. Ligand binding stepwise disrupts water network in thrombin: enthalpic and entropic changes reveal classical hydrophobic effect. *J. Med. Chem.* **2012,** *55,* 6094-6110.

(12) Geschwindner, S.; Ulander, J.; Johansson, P. Ligand binding thermodynamics in drug discovery: Still a hot tip? *J. Med. Chem.,* **2015,** *58,* 6321–6335.

(13) Klebe, G. The use of thermodynamic and kinetic data in drug discovery: decisive insight or increasing the puzzlement? *ChemMedChem.* **2015,** *10,* 229-231.

(14) Cusack K. P., Wang Y., Hoemann, M. Z., Marjanovic, J., Heym, R.G., Vasudevan, A. Design strategies to address kinetics of drug binding and residence time. *Bioorg. Med. Chem. Lett.* **2015,** *25,* 2019-2027.

(15) Margueron, R.; Justin, N.; Ohno, K.; Sharpe, M. L.; Son, J.; Drury, W. J.; Voigt, P.; Martin, S. R.; Taylor, W. R.; De Marco, V.; Pirrotta, V.; Reinberg, D.; Gamblin, S. J. Role of the polycomb protein EED in the propagation of repressive histone marks. *Nature* **2009,** *461,* 762-767.

(16) Morera, L; Lübbert, M; Jung, M. Targeting histone methyltransferases and demethylases in clinical trials for cancer therapy. *Clin. Epigenetics* **2016,** 8-57.

(17) He, Y; Selvaraju, S; Curtin, M. L.; Jakob, C. G.; Zhu, H.; Comess, K. M.; Shaw, B.; The, J.; Lima-Fernandes E.; Szewczyk, M., M.; Dong, C.; Klinge, K. L.; Li, H.; Pliushchev, M.; Algire, M. A.; Maag, D.; Guo, J.; Dietrich, J.; Panchal, S, C., Petros, A. M.; Sweis, R. F.; Torrent, M.; Bigelow, L. J.; Senisterra, G.; Li, F.; Kennedy, S.; Wu, Q.; Osterling D. J.; Lindley, D. J.; Gao, W.; Galasinski, S.; Barsyte-Lovejoy, D.; Vedadi, M.; Buchanan, F. G.; Arrowsmith, C. H.; Chiang, G. G.; Sun, C.; Pappano, W. N. The EED protein-protein interaction inhibitor A-395 inactivates the PRC2 complex. *Nat. Chem. Biol.* **2017,** *13,* 381-388.

(18) Qi, W.; Zhao, K.; Gu, J.; Huang, Y.; Wang, Y.; Zhang, H.; Zhang, M.; Zhang, J.; Yu, Z.; Li, L.; Teng, L.; Chuai, S.; Zhang, C.; Zhao, M.; Chan, H.; Chen, Z.; Fang, D.; Fei, Q.; Feng, L.; Feng, L.; Gao, Y.; Ge, H.; Ge, X.; Li, G.; Lingel, A.; Lin, Y.; Liu, Y.; Luo, F.; Shi, M.; Wang, L.; Wang, Z.; Yu, Y.; Zeng, J.; Zeng, C.; Zhang, L.; Zhang, Q.; Zhou, S.; Oyang, C.; Atadja, P.; Li, E. An allosteric PRC2 inhibitor targeting the H3K27me3 binding pocket of EED. *Nat. Chem. Biol.* **2017,** *13, 389-395.*

(19) Curtin, M. L.; Pliushchev, M. A.; Li, H.; Torrent, M.; Dietrich, J. D.; Jakob, C. G.; Zhu, H.; Zhao, H.; Wang, Y.; Ji , Z.; Clark, R. F.; Sarris, K. A.; Selvaraju, S.; Shaw, B.; Algire, M.

A.; He, Y.; Richardson, P. L.; Sweis, R. F.; Sun, C.; Chiang, G. G.; Michaelides, M. R. SAR of amino pyrrolidines as potent and novel protein-protein interaction inhibitors of the PRC2 complex through EED binding. *Bioorg. Med. Chem. Lett.* **2017**, *27,* 1576-1583.

(20) Yu, Z.; van Veldhoven, J. P. D.; Louvel, J.; 't Hart, I. M. E.; Rook, M. B.; van der Heyden, M. A. G.; Heitman, L. H.; IJzerman, A. P. Structure-affinity relationships (SARs) and structure-kinetics relationships (SKRs) of Kv11.1 blockers. *J. Med. Chem.* **2015,** *58,* 5916-5929.

(21) Stuckey, J. I.; Simpson, C.; Norris-Drouin, J. T.; Cholensky, S. H.; Lee, J.; Pasca, R.; Cheng, N.; Dickson, B. M.; Pearce, K. H.; Frye, S. V.; James, L. I. Structure-activity relationships and kinetic studies of peptidic antagonists of CBX chromodomains. *J. Med. Chem.* **2016,** *59,* 8913-8923.

(22) Miller, D. C.; Lunn, G.; Jones, P.; Sabnis, Y.; Daviesa, N. L.; Driscolla, P. Investigation of the effect of molecular properties on the binding kinetics of a ligand to its biological target. *Med. Chem. Commun.* **2012,** *3,* 449-452.

(23) Grüner, S.; Neeb, M.; Barandun, L. J.; Sielaff, F.; Hohn, C.; Kojima, S.; Steinmetzer, T.; Diederich, F.; Klebe, G. Impact of protein and ligand impurities on ITC-derived protein-ligand thermodynamics. *Biochim. Biophys. Acta* **2014,** *1840,* 2843-2850.

(24) Rühmann, E.; Betz, M.; Fricke, M.; Heine, A.; Schäfer, M.; Klebe, G. Thermodynamic signatures of fragment binding: Validation of direct versus displacement ITC titrations. *Biochim. Biophys. Acta* **2015,** *1850,* 647-656.

(25) Chodera, J. D.; Mobley, D. L. Entropy-enthalpy compensation: role and ramifications in biomolecular ligand recognition and design. *Annu. Rev. Biophys.* **2013,** *42,* 121-142.

(26) Malvern website whitepaper. Addressing the needs of drug discovery with the MicroCal PEAQ-ITC instruments. http://www.malvern.com/en/support/resource-center/Whitepapers/WP150130AddressingDrugDiscMicroCalPEAQ.aspx. (accessed March 29th, 2017)

(27) Brautigam, A. C. Fitting two- and three-site binding models to isothermal titration calorimetric data. *Methods.* **2015,** *76,* 124-136.

(28) One log unit change in K_D corresponds to ΔG (or ΔH or $-T\Delta S$) = 1.34 kcal/mole

(29) Freire, E. A thermodynamic approach to the affinity optimization of drug candidates. *Chem. Biol. Drug Des.* **2009,** *74,* 468-472.

(30) Berg, L.; Niemiec, M. S.; Qian, W.; Andersson, C. D.; Wittung-Stafshede, P.; Ekström, F.; Linusson, A. Similar but different: Thermodynamic and structural characterization of a pair of enantiomers binding to acetylcholinesterase. *Angew. Chem. Int. Ed.* **2012,** *51,* 12716-12720.

(31) Holdgate, G.; Geschwindner, S.; Breeze, A.; Davies, G.; Colclough, N.; Temesi, D.; Ward, L. Biophysical methods in drug discovery from small molecule to pharmaceutical. *Methods Mol. Biol.* **2013,** *1008,* 327-355.

(32) Edink, E.; Rucktooa, P.; Retra, K.; Akdemir, A.; Nahar, T.; Zuiderveld, O.; van Elk , R.; Janssen, E.; van Nierop, P.; van Muijlwijk-Koezen, J.; Smit, A. B.; Sixma, T. K.; Leurs, R.;

de Esch, I. J. Fragment growing induces conformational changes in acetylcholine-binding protein: a structural and thermodynamic analysis. *J. Am. Chem. Soc.* **2011**, *133,* 5363-5371.

(33) Winquist, J.; Geschwindner, S.; Xue, Y.; Gustavsson, L.; Musil, D.; Deinum, J.; Danielson, U. H. Identification of structural-kinetic and structural-thermodynamic relationships for thrombin inhibitors. *Biochemistry.* **2013,** *52,* 613-626.

(34) Klebe, G.; Applying thermodynamic profiling in lead finding and optimization. *Nat. Rev. Drug Discov.* **2015,** *14,* 95-110.

(35) Wilfong, E. M.; Du, Y.; Toone, E. J. An enthalpic basis of additivity in biphenyl hydroxamic acid ligands for stromelysin-1. *Bioorg. Med. Chem. Lett.* **2012**, 22, 6521-6524.

(36) Mollica, L.; Theret, I.; Antoine, M.; Perron-Sierra, F.; Charton, F.; Fourquez, J. M.; Wierzbicki, M.; Boutin, J. A.; Ferry, G.; Decherchi, S.; Bottegoni, G.; Ducrot, P.; Cavalli, A. Molecular dynamics simulations and kinetic measurements to estimate and predict protein-ligand residence times. *J. Med. Chem.* **2016,** *59,* 7167-7176.

Figure 1. Chemical structures of selected EED compounds.*

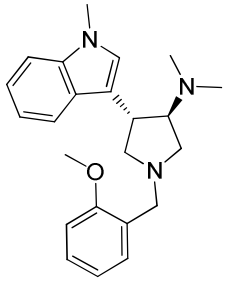

1

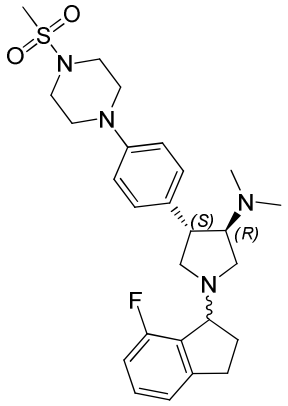

2

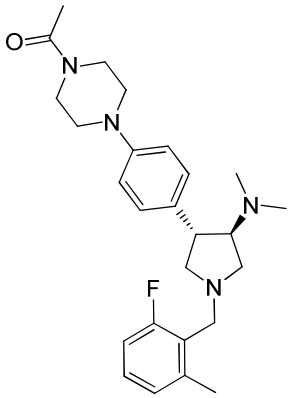

3

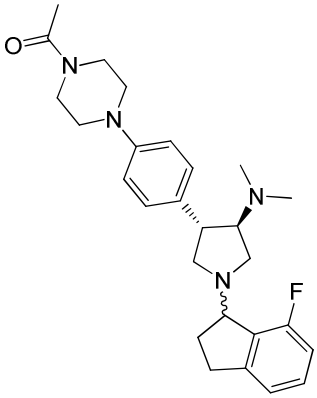

4

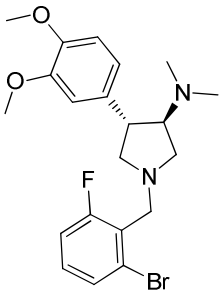

5

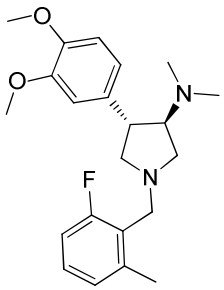

6

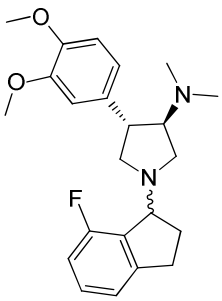

7

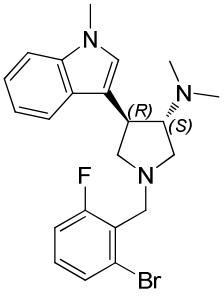

8

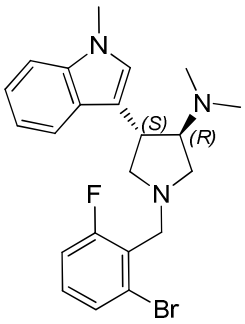

9

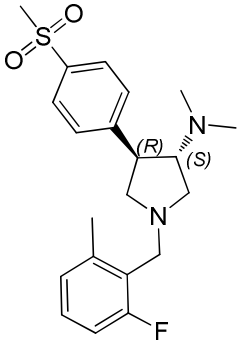

10

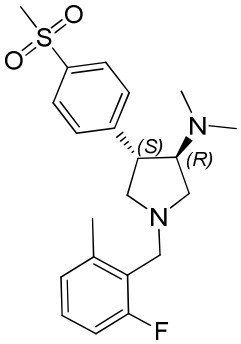

11

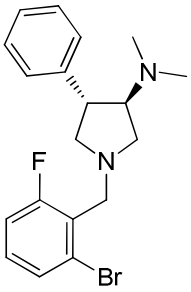

12

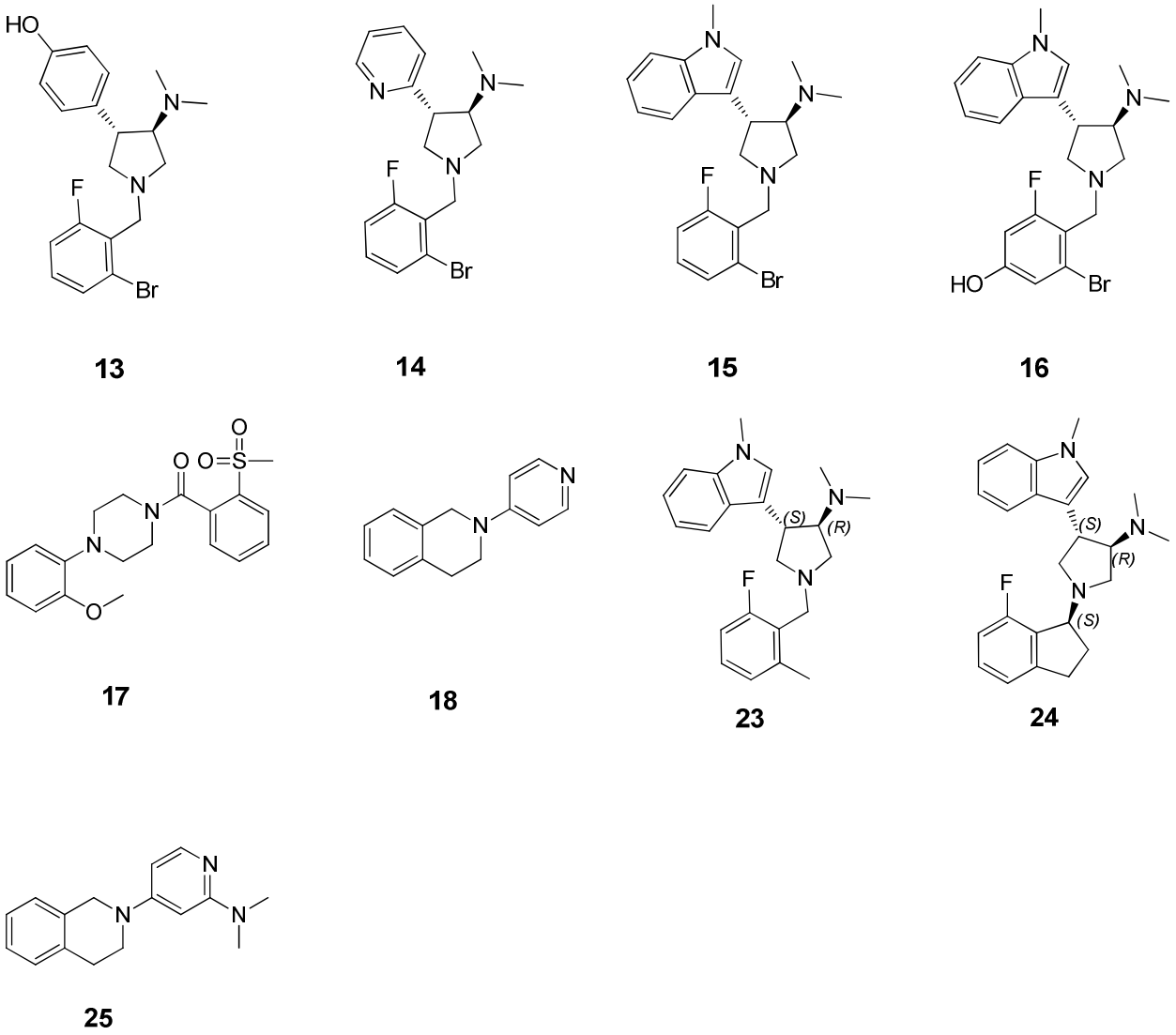

*Chiral centers were specified with absolute configurations.

Figure 2. Crystal structure of compound **1** bound to EED (PDB ID: 5U69)[19]

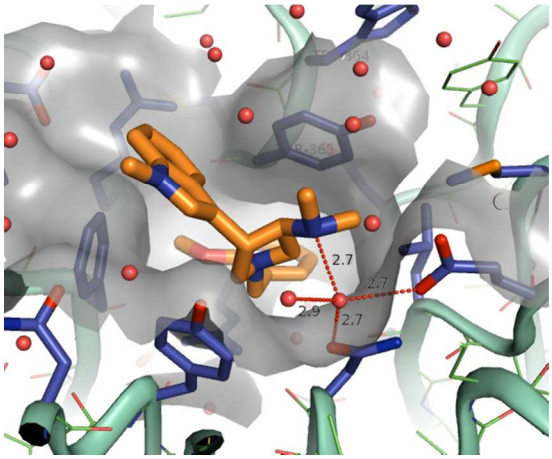

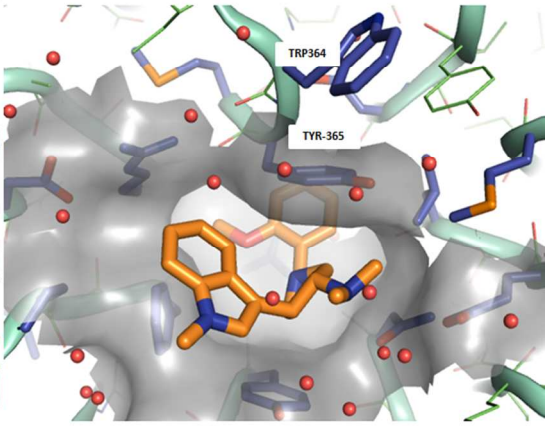

Figure 2a **Figure 2b**

Figure 3. Amino pyrrolidine SAR studies.

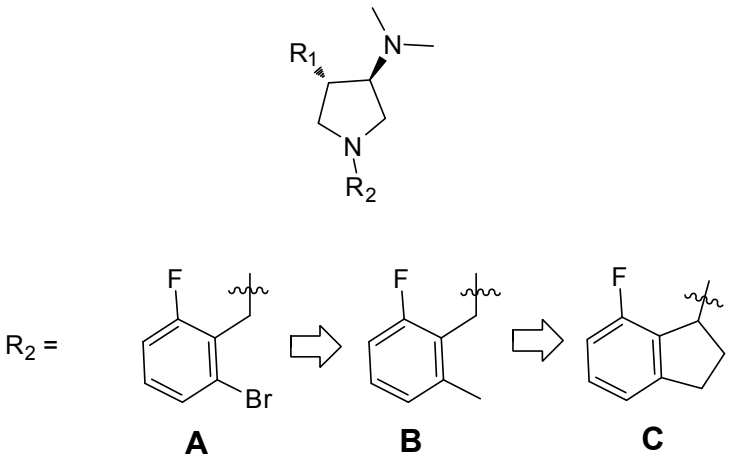

Figure 4. Correlation between SPR binding affinities K_D and TR-FRET binding affinities K_i (log scale plot)

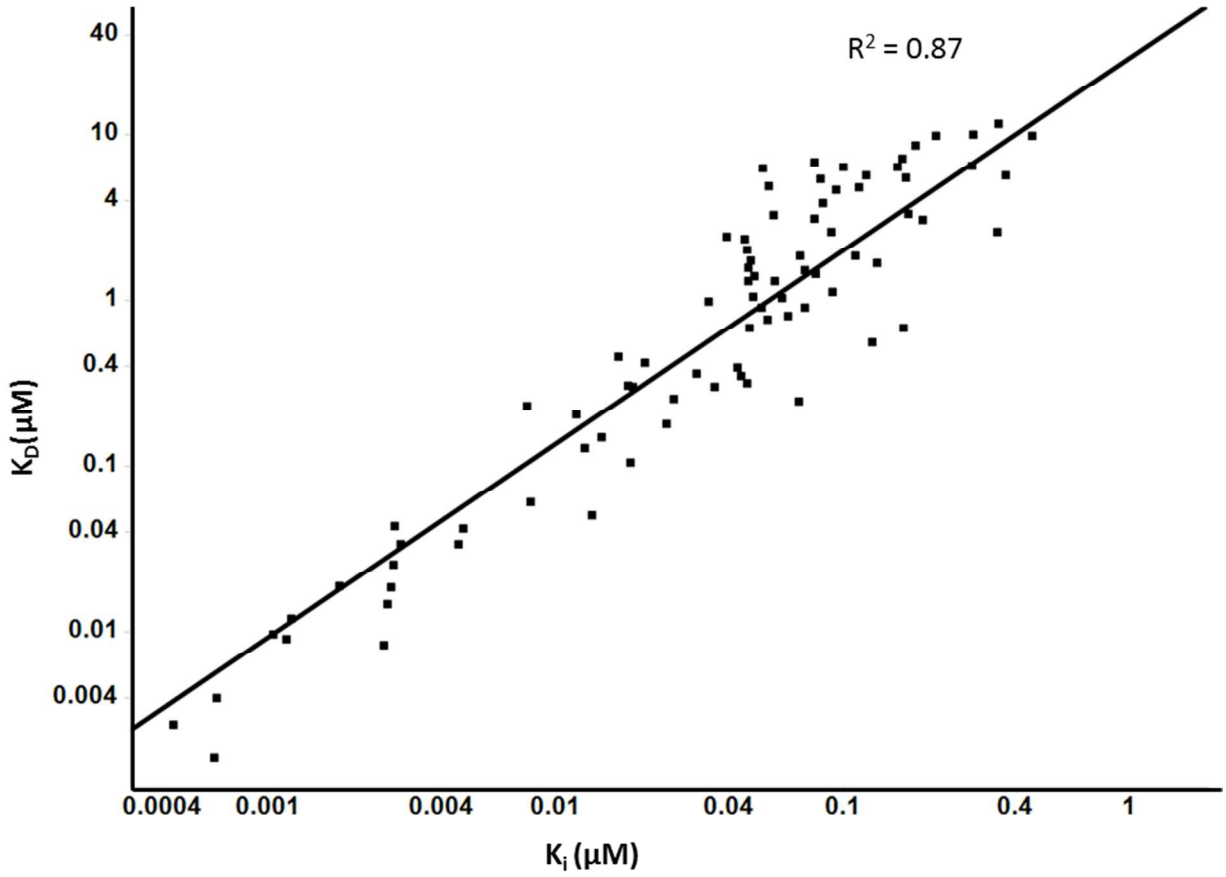

Figure 5. Kinetic plot of EED amino pyrrolidine compounds showing R_2 progression (log scale plot)

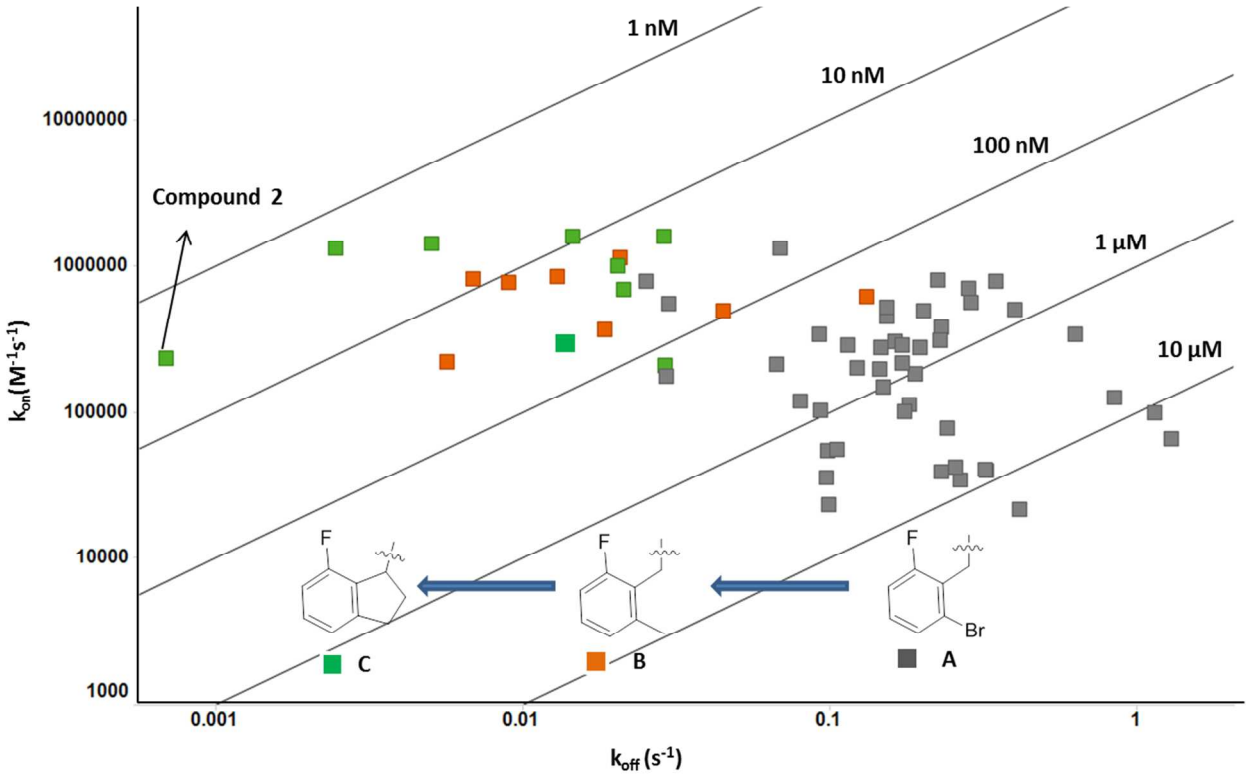

Table 1. Kinetic data of selected EED compounds

Compound	Ki (µM, TR-FRET)	k_{on} ($M^{-1}s^{-1}$)	k_{off} (s^{-1})	K_D (µM, SPR)
1	0.6	fast	fast	38
2	0.0003	1.6×10^6	0.003	0.002

3	0.003	1.1×10^{6}	0.02	0.02
4	0.0007	1.3×10^{6}	0.005	0.004
5	0.018	3.1×10^{5}	0.11	0.30
6	0.012	6.0×10^{5}	0.12	0.21
7	0.003	3.3×10^{5}	0.015	0.043
8	0.08	fast	fast	3.10
9	0.01	1.9×10^{5}	0.03	0.15
10	0.29	fast	fast	1.4
11	0.01	7.3×10^{5}	0.1	0.14

12	0.11	fast	fast	4.8
13	0.091	fast	fast	2.6
14	0.45	fast	fast	9.8
15	0.02	2.1×10^5	0.07	0.31
16	0.008	2.5×10^5	0.02	0.061
17	1.5	fast	fast	13.4
18	0.95	fast	fast	22

Table 2. The influence of compound chirality on ITC K_D. *

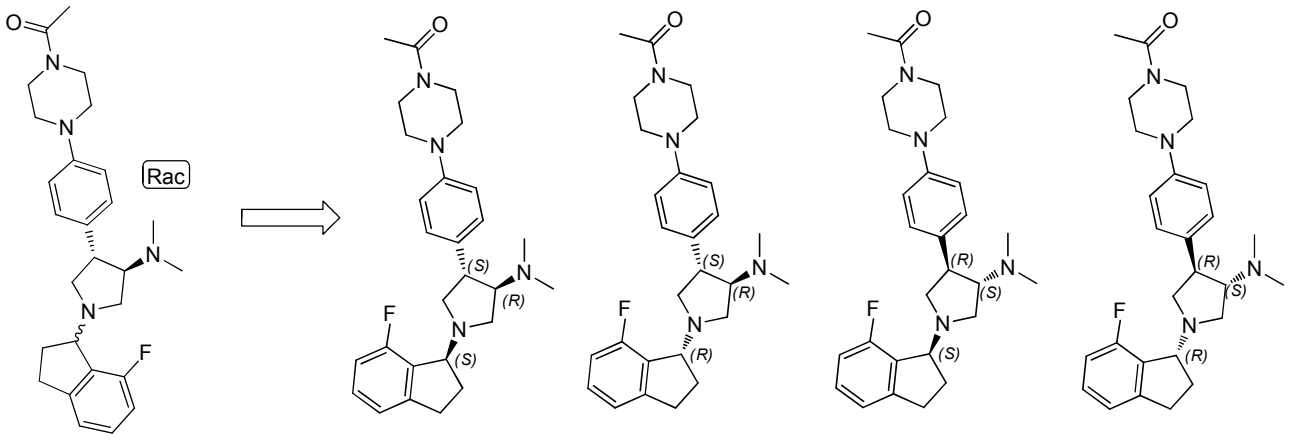

Compound	Ki (μM)-TR-FRET	K_D (μM) - SPR	K_D (μM) - ITC	ΔH (cal/mol)	-TΔS (cal/mol)
4	0.0007	0.004	2.1	-22900	15138
19	0.0003	0.001	0.01	- 18800	7867
20	0.003	0.10	1.14	-15800	7629
21	0.042	0.29	2.2	-11780	4053
22	0.018	0.20	0.11	-16000	6496

*Compound **20** is contaminated by ~5% compound **19** and compound **21** is contaminated with ~5% compound **20** and **22.**

Table 3. Thermodynamic data of selected EED compounds

Compound	Ki (μM)-TR-FRET	K_D (μM) -ITC	ΔH (cal/mol)	-TΔS (cal/mol)
23	0.004	0.006	-18200	7033
24	0.001	0.01	-20100	9208
8	0.08	0.37	-16000	7510
9	0.01	0.09	-16900	7301
10	0.29	0.94	-14400	6139
11	0.01	0.03	-15500	5334
18	0.95	5.2	-9570	2360
25	0.68	2.5	-15530	7867

Figure 6. Box Plot of K_i, k_{off} and k_{on} to cellular activity (x-axis). Cellular activity is binned into three categories: less than 0.1 µM; between 0.1 to 1 µM and above 1 µM. Box plots show minimum and maximum values as whiskers; the 25th, 50th, and 75th percentiles as boxes; and mean values as crosses.

Figure 6a

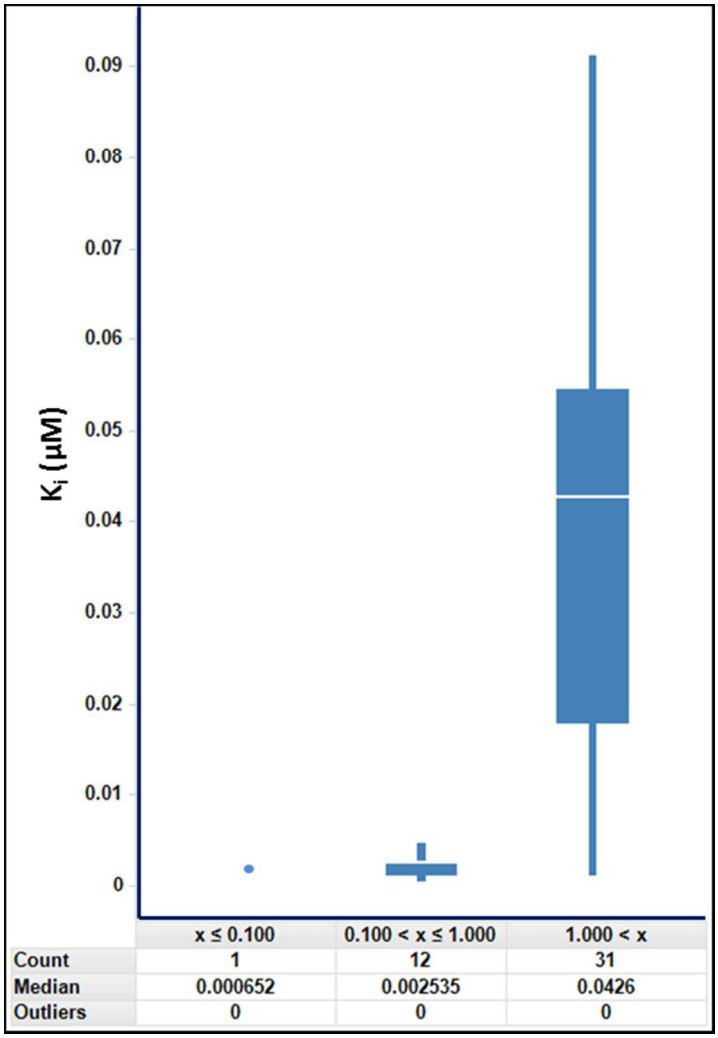

Figure 6b

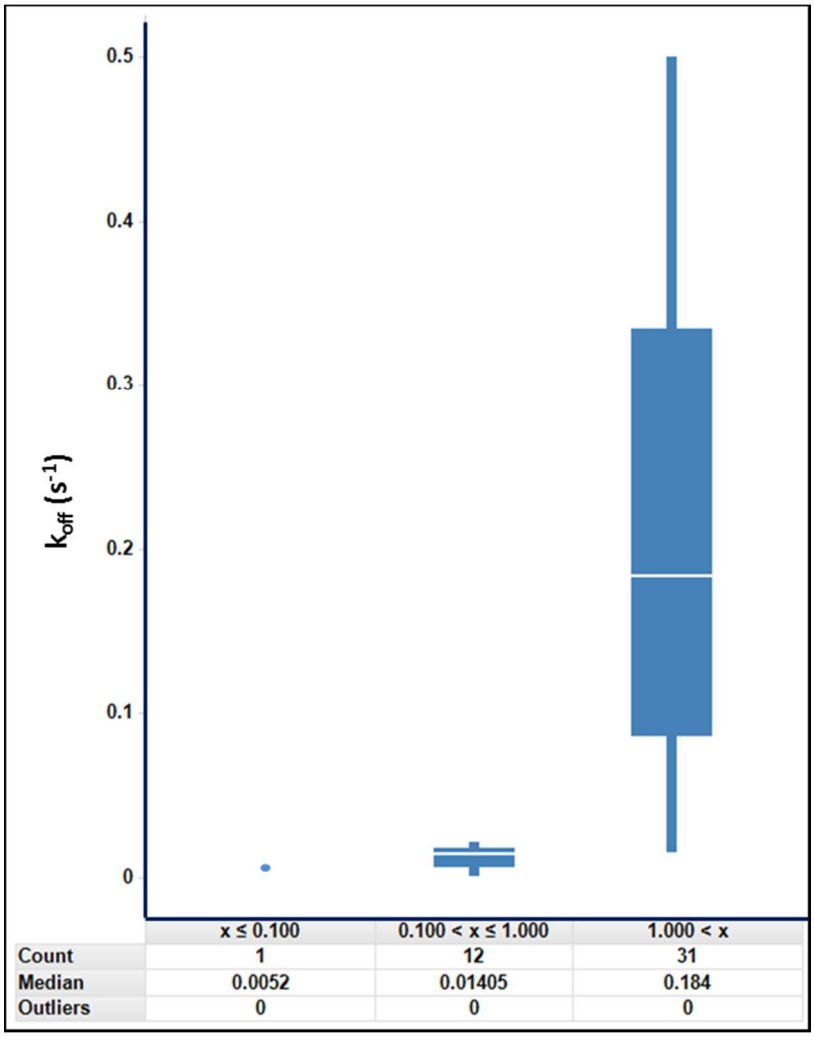
0.5
0.4
0.3
0.2
0.1
0
k_{off} (s^{-1})
x ≤ 0.100
0.100 < x ≤ 1.000
1.000 < x
Count 1 12 31
Median 0.0052 0.01405 0.184
Outliers 0 0 0

Figure 6c

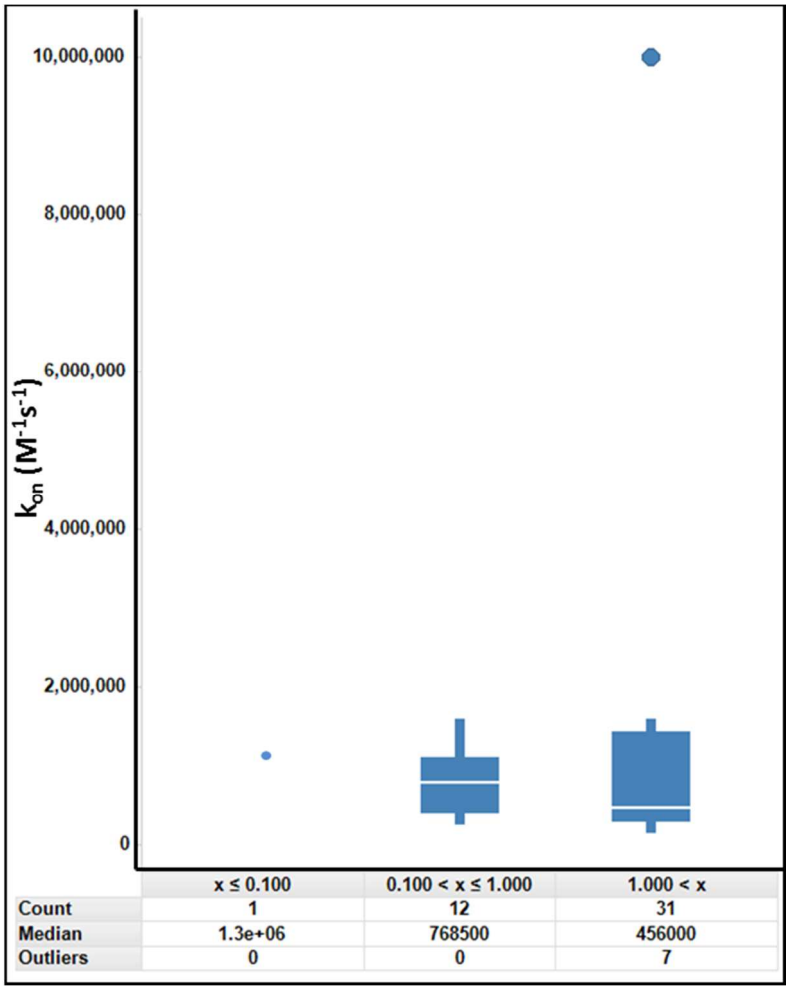

Figure 7. Plot of ITC binding affinities K_D to TR-FRET binding affinities K_i for 7-fuloroindanyl compounds

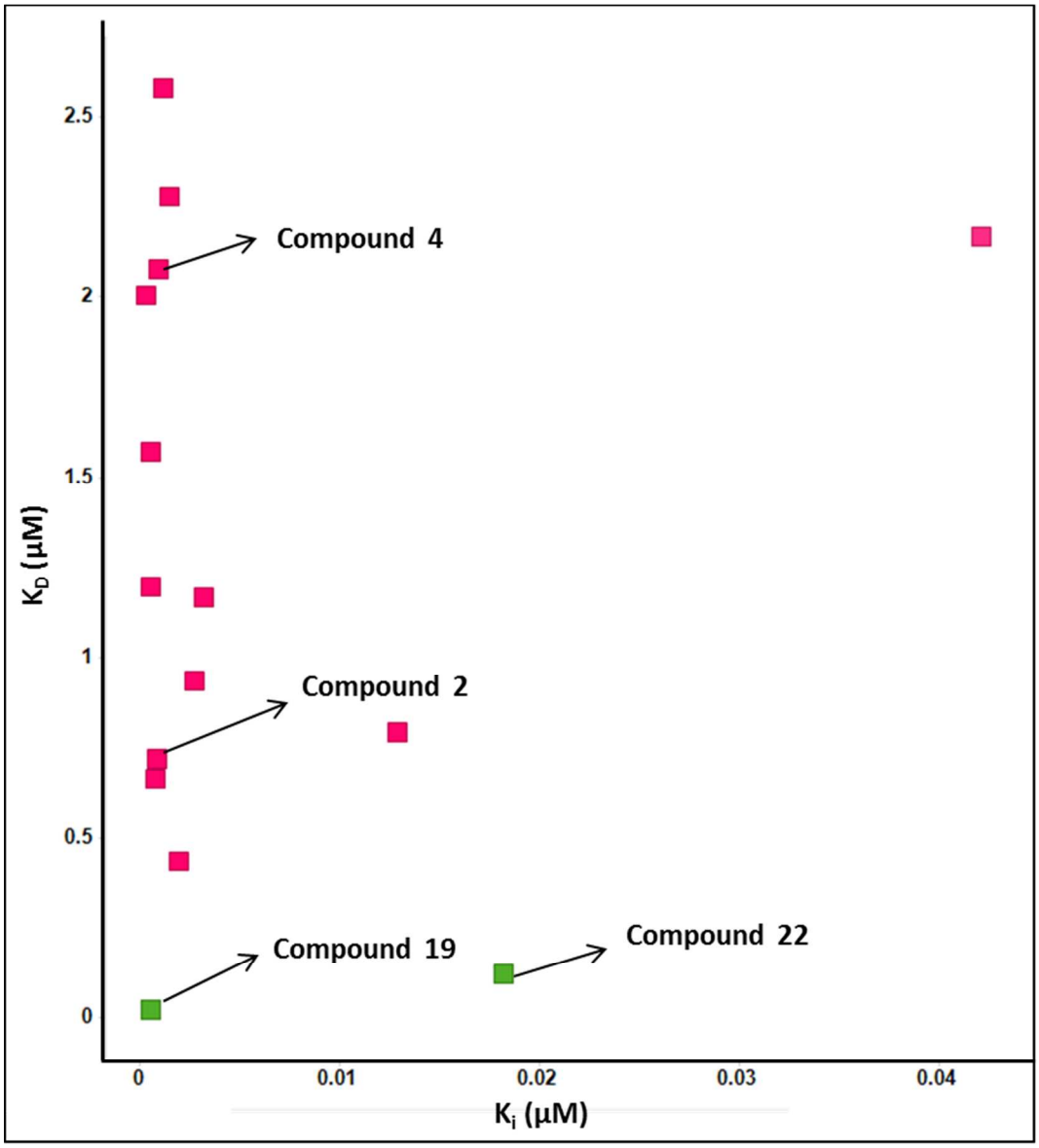

Figure 8. Plot of ITC binding affinities K_D to TR-FRET binding affinities K_i for chirally pure compounds (ee > 95%, log scale plot, Figure **1**).

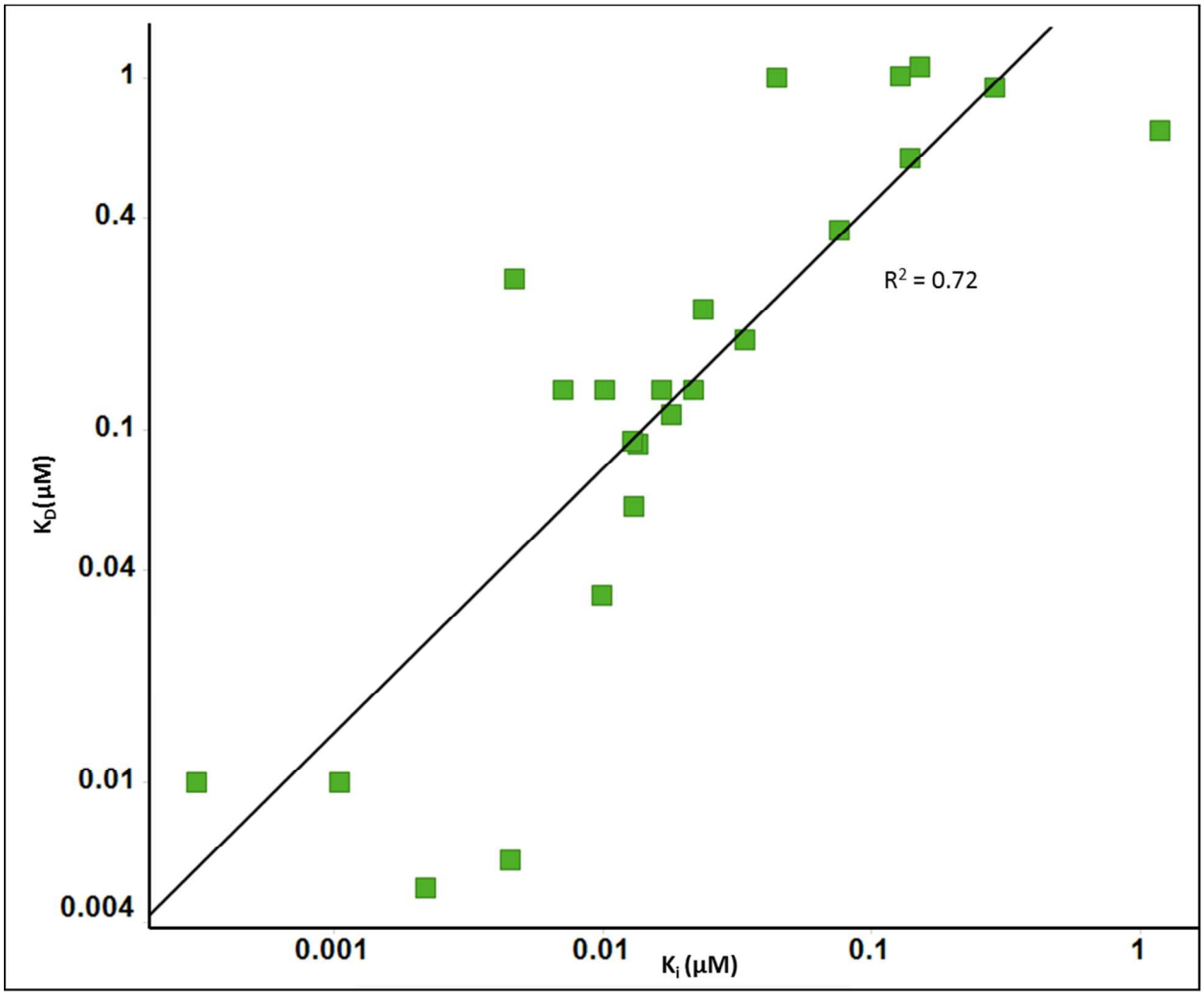

Figure 9. Thermodynamic Plot for chirally pure EED aminopyrrolidine compounds (ee > 95%)

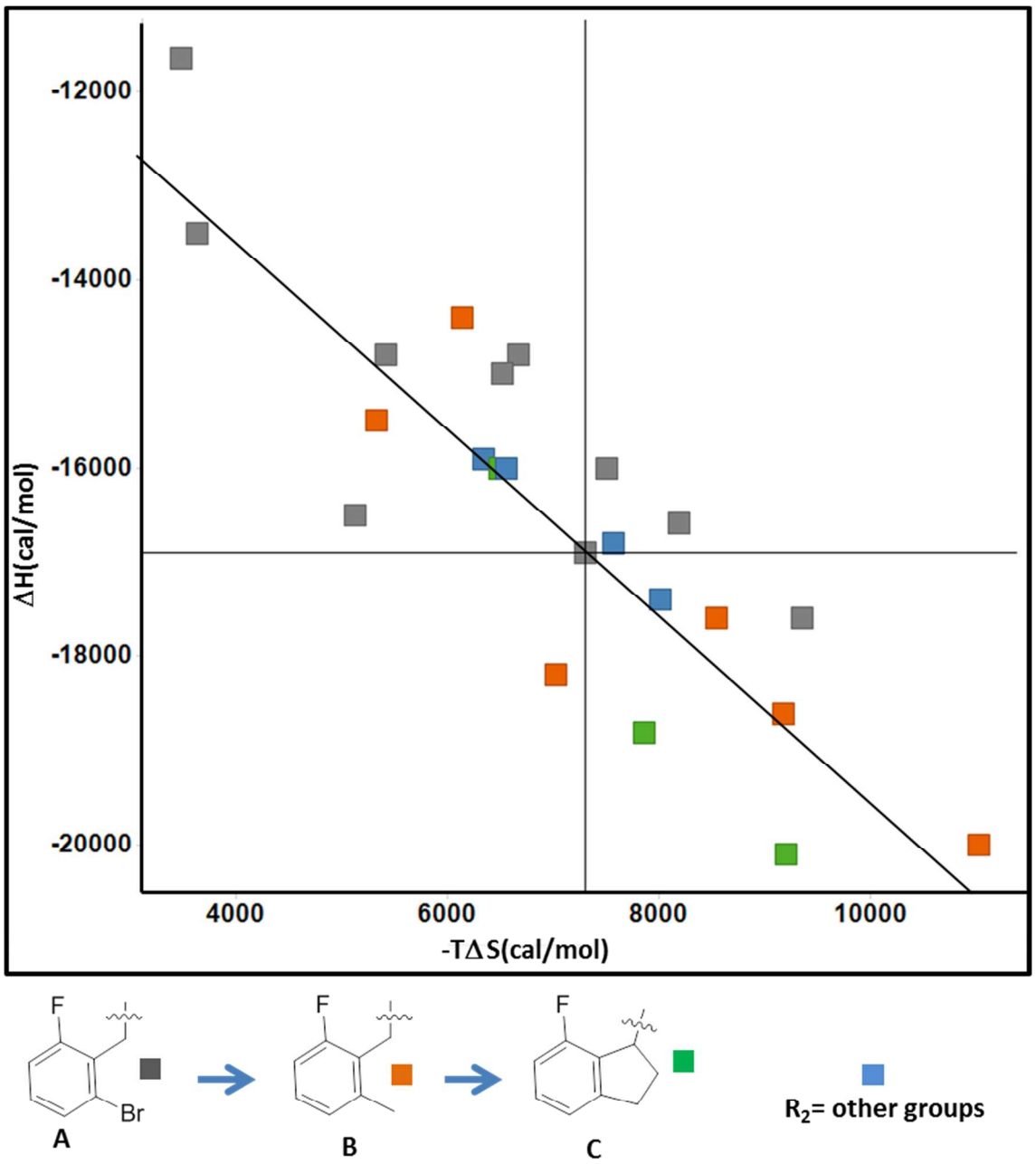

Table of Contents Graphic

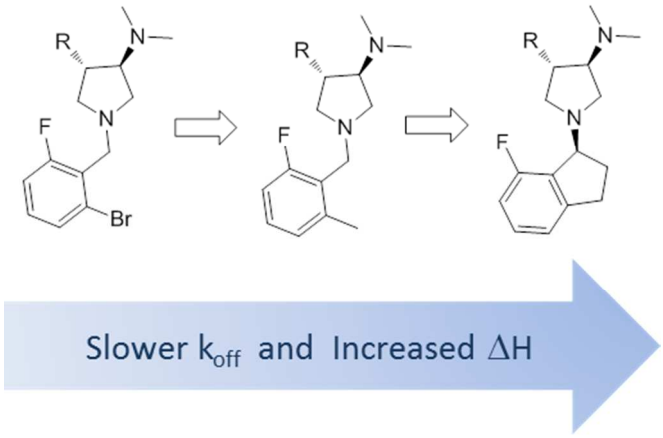
R
N
F
N
Br
R
N
F
N
R
N
F
N
Slower k_{off} and Increased ΔH